



# Coordinated U–Pb geochronology, trace element, Ti-in-zircon thermometry and microstructural analysis of Apollo zircons

Carolyn A. Crow<sup>a,b,\*</sup>, Kevin D. McKeegan<sup>a</sup>, Desmond E. Moser<sup>c</sup>

<sup>a</sup> Department of Earth, Planetary, and Space Sciences, University of California, Los Angeles, Los Angeles, CA 90095, USA

<sup>b</sup> Nuclear and Chemical Sciences Division, Lawrence Livermore National Laboratory, Livermore, CA 94550, USA

<sup>c</sup> Department of Earth Sciences, University of Western Ontario, London, Ontario N6A 5B7, Canada

Received 29 April 2016; accepted in revised form 13 December 2016; available online 28 December 2016

## Abstract

We present the results of a coordinated SIMS U–Pb, trace element, Ti-in-zircon thermometry, and microstructural study of 155 lunar zircons separated from Apollo 14, 15, and 17 breccia and soil samples that help resolve discrepancies between the zircon data, the lunar whole rock history and lunar magma ocean crystallization models. The majority of lunar grains are detrital fragments, some nearly 1 mm in length, of large parent crystals suggesting that they crystallized in highly enriched KREEP magmas. The zircon age distributions for all three landing sites exhibit an abundance of ages at ~4.33 Ga, however they differ in that only Apollo 14 samples have a population of zircons with ages between 4.1 and 3.9 Ga. These younger grains comprise only 10% of all dated lunar zircons and are usually small and highly shocked making them more susceptible to Pb-loss. These observations suggest that the majority of zircons crystallized before 4.1 Ga and that KREEP magmatism had predominantly ceased by this time. We also observed that trace element analyses are easily affected by contributions from inclusions (typically injected impact melt) within SIMS analyses spots. After filtering for these effects, rare-earth element (REE) abundances of pristine zircon are consistent with one pattern characterized by a negative Eu anomaly and no positive Ce anomaly, implying that the zircons formed in a reducing environment. This inference is consistent with crystallization temperatures based on measured Ti concentrations and new estimates of oxide activities which imply temperatures ranging between  $958 \pm 57$  and  $1321 \pm 100$  °C, suggesting that zircon parent magmas were anhydrous. Together, the lunar zircon ages and trace elements are consistent with a  $\leq 300$  My duration of KREEP magmatism under anhydrous, reducing conditions. We also report two granular texture zircons that contain baddeleyite cores, which both yield  $^{207}\text{Pb}$ – $^{206}\text{Pb}$  ages of 4.33 Ga. These grains are our best constraints on impact ages within our sample population, and suggest at least one large impact is contemporaneous with the most common time of magmatic zircon formation on the Moon's crust visited by the Apollo missions. © 2017 Elsevier Ltd. All rights reserved.

**Keywords:** Apollo; Lunar zircon; Late heavy bombardment; KREEP; Trace elements; Ti-in-zircon thermometry; Microstructures

## 1. INTRODUCTION

The residual melts of the global lunar magma ocean (LMO) are thought to have been highly enriched in K, the Rare Earth Elements, and P (KREEP), (Warren and Wasson, 1979) in addition to other incompatible elements, such as Zr, Th, and U, making KREEP magmas the most

\* Corresponding author at: Nuclear and Chemical Sciences Division, Lawrence Livermore National Laboratory, Livermore, CA 94550, USA.

E-mail address: [crow7@llnl.gov](mailto:crow7@llnl.gov) (C.A. Crow).

likely source for the zircons observed in Apollo samples (Meyer et al., 1971; Dickinson and Hess, 1982). As such, the lunar zircons have been used to infer the timing and characteristics of KREEP magmatism, and their ability to record ages of secondary impact events has made them useful in investigating the chronology of impacts on the early Moon (e.g. Nemchin et al., 2008, 2009; Grange et al., 2009, 2011, 2013b; Taylor et al., 2009a).

Most available data on lunar zircons are from Apollo 14 and 17 landing sites. These zircons exhibit a range of crystallization ages from 3.88 to 4.42 Ga, suggesting that the Moon experienced long-lived KREEP magmatism that lasted for up to ~500 Myr (e.g. Meyer et al., 1989; Nemchin et al., 2009; Taylor et al., 2009a, 2009b; Hopkins and Mojzsis, 2015). This is much longer than the maximum solidification timescale of ~220 Myr inferred from LMO crystallization models (Meyer et al., 2010; Elkins-Tanton et al., 2011). Zircons from both Apollo 14 and 17 landing sites exhibit a common peak in their age distributions around ~4.33 Ga, however, they differ in that the younger (<4.1 Ga) population is missing in the Apollo 17 samples. Contraction of one large KREEP reservoir has been invoked to explain this dichotomy (Nemchin et al., 2008).

Both terrestrial and lunar zircons have been shown to record signatures of impact/shock metamorphism (e.g. Krogh et al., 1993; Moser et al., 2011; Timms et al., 2012; Grange et al., 2013a, 2013b). In cases of complete recrystallization or growth in an impact environment, the zircon ages are thought to reflect the age of the associated impact (e.g. Gibson et al., 1997; Moser, 1997). Based on impact recrystallized or altered zircons in the Apollo collection, it has been proposed that multiple basin-sized impacts occurred prior to the period of the so-called “late heavy bombardment” (LHB) (Nemchin et al., 2008; Grange et al., 2009, 2011; Norman and Nemchin, 2014).

It has also been suggested that variability in lunar zircon REE concentrations, both relative and absolute, may be used to infer zircon provenance (Nemchin et al., 2010). Previous studies have identified some lunar zircons that exhibit positive Ce anomalies, which is characteristic of crystallization from oxidized magmas (Nemchin et al., 2010; Trail et al., 2012; Hopkins and Mojzsis, 2015). Another indicator of parent melt conditions is Ti-in-zircon crystallization temperature. While these temperatures are generally higher for lunar samples than for their terrestrial counterparts, some lunar zircons appear to record crystallization temperatures that would be below the dry solidus for basaltic or granitic compositions. These low temperatures would imply that some lunar grains formed in slightly hydrated conditions, which is contrary to the understanding of the early lunar magmatic evolution that has developed based on the whole rock record that suggests dry and reducing conditions (Valley et al., 2014).

In this paper, we present results from a coordinated geochronologic, microstructural, and compositional survey of 155 lunar zircons from the Apollo 14, 15, and 17 landing sites. Zircon U–Pb ages, trace elements, and Ti-in-zircon temperatures are combined with shock microstructural information to address the timing and compositional diversity of residual KREEP magmatism. With this comprehen-

sive study, we investigate the variations in zircon crystallization histories between three Apollo landing sites, re-evaluate the evidence for oxidizing and hydrous conditions, and examine the influence of secondary, shock-related processes on both the zircon trace element and age analyses. Pairing the zircon crystallization and impact chronologies with trace element information may lead to a more robust understanding of the evolution of early lunar magmatic systems.

## 2. SAMPLE DESCRIPTION

Zircon grains were separated from three soil and six breccia samples, which were chosen based on high Zr content (see Appendix A) and/or previously published zircon yields. Although extraction of zircon does not allow for petrographic information to be interpreted, most lunar zircons that have been discovered in Apollo thin sections are either detrital igneous grains or have textures suggestive of growth in an impact environment (Meyer et al., 1989, 1996; Pidgeon et al., 2007; Nemchin et al., 2008, 2009, 2010; Taylor et al., 2009a; Grange et al., 2011, 2013a, 2013b; Hopkins and Mojzsis, 2015). A compositional understanding of the host rock from which the zircons were extracted is not imperative for this study; however, sample descriptions are provided here for completeness including relevant ages.

### 2.1. Soil 14163

Sample 14163 is a sub-mature soil collected nearby the Apollo 14 lunar module and is characterized by a large KREEP component and high percentage of glass (Morris, 1978; Labotka et al., 1980; Simon and Papike, 1981).

### 2.2. Soil 14259

Sample 14259 was collected from the top 1 cm of soil to the west of the Apollo 14 lunar module. The sample is a mature soil with a high concentration of agglutinates (Von Engelhardt et al., 1972; McKay et al., 1972). The agglutinates separated from soil 14259 exhibit discordant behavior suggestive of Pb-loss at ~400 Ma (Church et al., 1976). This recent Pb-loss event may be associated with formation of Cone Crater, which has been dated at  $24.4 \pm 1.1$  Ma (Drozd et al., 1974). Exposure ages of this sample were determined from the  $^{236}\text{U}/^{238}\text{U}$  ratio and  $^{126}\text{Xe}$  concentrations due to Ba spallation, which yielded ages of 450 Ma and 550 Ma, respectively (Burnett et al., 1972; Fields et al., 1973).

### 2.3. Breccia 14304

Sample 14304 is a clast-rich impact melt breccia with a crystallized matrix (McGee et al., 1979). Shih et al. (1987) determined Rb/Sr ages of very high potassium (VHK) basalt clasts of  $3.95 \pm 0.04$  and  $3.99 \pm 0.02$  Ga and a Sm/Nd age  $4.04 \pm 0.11$  Ga. Snyder et al. (1995) found older Rb/Sr and Sm/Nd ages for alkali anorthosite clasts of  $4.336 \pm 0.081$  and  $4.108 \pm 0.053$  Ga, respectively.

#### 2.4. Breccia 14305

Sample 14305 is a Fra Mauro breccia collected near the Apollo 14 lunar module. Like 14304, this sample is a clast-rich, crystalline matrix breccia. It has high concentrations of both KREEP and meteoritic material (Wanke et al., 1972; Palme et al., 1978), and highland gabbroic anorthosite, pink spinel, apatite and zircons have all previously been identified (Dence and Plant, 1972; Lovering et al., 1972). The Rb–Sr analyses yield both a young whole rock age of  $3.83 \pm 0.08$  Ga and an older clast age of  $4.23 \pm 0.05$  Ga (olivine gabbroanorthite) (Taylor et al., 1983; Shih et al., 1986). Three papers have previously reported U–Pb and  $^{207}\text{Pb}$ – $^{206}\text{Pb}$  ages of zircons from 14305, with ages ranging between 3.97 and 4.35 Ga (Hinton and Meyer, 1991; Nemchin et al., 2008; Taylor et al., 2009a,b). The  $^{81}\text{Kr}$ –Kr exposure age of 14305 is  $27.6 \pm 1.5$  Ma (Eugster et al., 1984).

#### 2.5. Breccia 14321

This sample was collected from the edge of Cone Crater and is thought to be part of the Fra Mauro Formation (Swann et al., 1971, 1977; Wilshire and Jackson, 1972). It is a clast-rich (about 30%), crystalline matrix breccia that contains anorthositic clasts considered pristine based on their very low Ir concentrations (Simonds et al., 1977; Warren et al., 1981). There have been two studies of the exposure ages of sample 14321:  $24 \pm 2$  Ma by the  $^{38}\text{Ar}$  method and 27 Ma by the  $^{81}\text{Kr}$  method (Burnett et al., 1972; Lugmair and Marti, 1972). Burnett et al. (1972) interpret this to be the age of Cone Crater, near which the samples were collected.

Small zircons were identified in multiple thin sections by Grieve et al. (1975), and Braddy et al. (1975) measured U concentrations of 93 zircons from sample 14321 by counting fission tracks and determined a median concentration of 50 ppm. Meyer et al. (1996) and Nemchin et al. (2008, 2006) measured the U–Pb ages of zircons in thin section by sensitive high-resolution ion microprobe (SHRIMP). The  $^{207}\text{Pb}$ – $^{206}\text{Pb}$  ages range between 3.89 and 4.40 Ga. Nemchin et al. (2006) also measured the oxygen isotopes of 14 of these zircons and found their  $\delta^{18}\text{O}$  to be within error of terrestrial mid-ocean ridge basalts. Taylor et al. (2009a, 2009b) reported  $^{207}\text{Pb}$ – $^{206}\text{Pb}$  ages of zircons separated from 14321 rock cuttings, which are consistent with previous studies. They also reported initial  $^{176}\text{Hf}/^{177}\text{Hf}$  ratios that suggest a separation/formation age of the KREEP reservoir of  $4.478 \pm 0.046$  Ga ( $1\sigma$ ).

#### 2.6. Soil 15311

Soil 15311 is a rake sample collected from the rim of Spur Crater, a small  $\sim 100$  m crater on the edge of the Apennine front. The Apennine Mountains are located on the southeastern edge of the Imbrium basin and are thought to have formed partially due to uplift from the basin-forming impact (Swann et al., 1972; Heiken et al., 1991). Soil 15311 has REE compositions suggestive of a KREEP basalt component (Korotev, 1987).

#### 2.7. Breccia 15405

Sample 15405 is a KREEP-rich breccia collected from a large boulder  $\sim 250$  m from Spur Crater (Swann et al., 1972). The clast population is dominated by KREEP basalt, with a few quartz monzodiorite (QMD), granite, and other clasts. Ar–Ar analyses of a QMD clast give a poorly defined mid-temperature plateau Ar–Ar age of  $1.272 \pm 0.016$  Ga (Bernatowicz et al., 1978; age corrected for new decay constant of Renne et al., 2011), which is in agreement with the lower intercept of the U–Pb concordia diagram for zircons in the QMD clast. The two zircon concordia intercepts are  $4.294 \pm 0.026$  and  $1.320 \pm 0.250$  Ga (Meyer et al., 1996). The older age is interpreted as the age of zircon formation and the younger age is thought to be the breccia formation age. An additional 11 zircons and 13 apatite grains in 15405 thin sections were dated by Grange et al. (2013b) and also appear to be affected by a young Pb-loss event at  $1938 \pm 96$  Ma.

#### 2.8. Breccia 15455 with Shocked Norite

Sample 15455 was also collected from the rim of Spur Crater and consists of older shocked norite surrounded by a younger dark impact melt breccia. Shih et al. (1993) measured Rb/Sr and Sm/Nd ages of  $4.59 \pm 0.13$  and  $4.53 \pm 0.29$  Ga for norite clasts. The rock fragments obtained for this study contain both lithologies.

#### 2.9. Breccia 72275

Sample 72275 is a feldspathic breccia that may represent ejecta from Serenitatis basin (Dalrymple and Ryder, 1996). This breccia has a high abundance of KREEPy non-mare basalt, and as a result has high concentrations of trace elements (Blanchard et al., 1975). Shih et al. (1992) reported Rb–Sr and Sm–Nd ages for a KREEP basalt clast of  $4.31 \pm 0.08$  and  $4.08 \pm 0.07$  Ga, respectively. Zircons have previously been reported in 72275 and have  $^{207}\text{Pb}$ – $^{206}\text{Pb}$  ages ranging from 4.24 to 4.42 Ga (Nemchin et al., 2008, 2009).

### 3. ANALYTICAL TECHNIQUES

#### 3.1. Sample preparation

Our sample preparation techniques follow those outlined in Taylor et al. (2009a), in which zircons were mechanically separated from breccia and soil samples by using a combination of hand crushing in an agate mortar, heavy-liquid mineral separation, and hand picking zircon grains. Although petrographic information is lost, the advantage of the separation technique is it allows for larger numbers and larger sizes of zircons to be recovered. No acicular fragments were obvious in our samples, however, preservation of delicate acicular zircons may be problematic during the crushing process, a factor that must be considered when evaluating the abundance of impact grown samples in our dataset.

After hand-picking, zircons were positively identified by using energy-dispersive X-ray spectroscopy (EDS) in the UCLA Tescan Scanning Electron Microscope (SEM) and then mounted in epoxy rounds. Each round was minimally polished with silicon carbide disks to expose a flat surface of the zircon necessary for SEM imaging and secondary ion mass spectrometry (SIMS) analyses. Maximizing retention of material during polishing was a necessity for later noble gas analyses (Crow et al., 2015).

### 3.2. SEM and SIMS measurements

All mounted zircons were imaged by secondary electron (SE), backscattered electron (BSE) and cathodoluminescence (CL) to characterize zoning, inclusions, fractures, and recrystallization textures. Selected samples were vibratory polished in a solution of colloidal 0.05  $\mu\text{m}$  alumina and neutral water and analyzed by electron backscatter diffraction (EBSD) at the Zircon and Accessory Phase (ZAP) Lab at the University of Western Ontario to search for evidence of recrystallization and other shock features.

U–Pb and REE concentrations were determined with the UCLA CAMECA *ims1270* ion microprobe during multiple sessions between 2009 and 2014. U–Pb ages,  $^{207}\text{Pb}$ – $^{206}\text{Pb}$  ages, and U concentrations were measured with  $\sim 20$ – $40 \mu\text{m}$  spots using the protocols described in Mojzsis et al. (2003). Ages and concentrations were calibrated against the AS3 zircon age standard and 91500 zircon U standard, respectively (Paces and Miller, 1993; Wiedenbeck et al., 2004). A  $^{204}\text{Pb}$  correction was made to account for common Pb contamination, but in most cases  $^{204}\text{Pb}$  was not detected. All of the lunar zircons have Pb that is above 97% radiogenic and the majority of grains are  $\geq 99\%$  radiogenic, so the U–Pb and  $^{207}\text{Pb}$ – $^{206}\text{Pb}$  ages reported here are not affected by choice of using either a terrestrial or lunar Pb isotopic composition for the  $^{204}\text{Pb}$  correction (Taylor et al., 2009a, 2009b). The most likely source of Pb contamination is from sample preparation; we therefore chose a common Pb composition of southern California surface waters for this correction (Sañudo-Wilhelmy and Flegal, 1994).

Trace elements, including REE, Ti, Hf, Th, U, and Fe were measured in peak switching mode, following the protocol described by Bell and Harrison (2013). Sensitivity factors were calibrated from analyses of four NIST standard glasses and the 91500 zircon standard.

## 4. RESULTS

We recovered 117 zircons from Apollo 14 samples, 42 zircons from Apollo 15 samples, and 12 from the Apollo 17 samples. Fig. 1A shows examples of typical lunar zircons from this study. Lunar grains differ from their terrestrial counterparts in that lunar zircons are rarely euhedral except for grains with granular texture recrystallization (see Fig. 2). CL imaging of the lunar grains also suggests that the majority are pieces of larger original zircons fragmented during subsequent impact events, and some fragments can be up to  $\sim 1 \text{ mm}$  in diameter (Fig. 1B–D).

### 4.1. U–Pb and $^{207}\text{Pb}$ – $^{206}\text{Pb}$ ages

We measured U–Pb and  $^{207}\text{Pb}$ – $^{206}\text{Pb}$  ages for 155 lunar zircons (the data are reported in Appendix A). We note that some small zircons were lost during removal of coatings or polishing between multiple sessions of SEM imaging and SIMS analyses, and for these grains we have only images and/or trace element analyses, but no age information. The results of our age analyses are shown as histograms in Fig. 3 along with ages reported in previous Apollo zircon studies. Fig. 3 was produced using the oldest  $^{207}\text{Pb}$ – $^{206}\text{Pb}$  age measured for each zircon, which is a lower limit on the igneous age, in order to illustrate the range of igneous ages recorded by the Apollo zircons (grains with impact growth or recrystallization textures were excluded in this figure and are discussed in 5.1.2).

Apollo 14 zircons exhibit the largest range in  $^{207}\text{Pb}$ – $^{206}\text{Pb}$  ages spanning from  $3942 \pm 9$  to  $4408 \pm 3 \text{ Ma}$  ( $1\sigma$ ), whereas Apollo 15 and 17 zircon ages are between  $4101 \pm 14 \text{ Ma}$  and  $4378 \pm 10 \text{ Ma}$  ( $1\sigma$ ). The two  $< 4.1 \text{ Ga}$  ages from Apollo 15 are both from zircons that are highly discordant and show evidence of recent Pb-loss, so there is a possibility that their  $^{207}\text{Pb}$ – $^{206}\text{Pb}$  ages are also disturbed (Meyer et al., 1996; Grange et al., 2013b). Despite the variation in the range of  $^{207}\text{Pb}$ – $^{206}\text{Pb}$  ages, all of the landing sites show a large abundance of grains with ages between 4320 and 4350 Ma; 80% of Apollo 17 zircons,  $\sim 50\%$  of Apollo 15, and  $\sim 20\%$  of Apollo 14 zircons analyzed fall within this age range. Most of the zircons are concordant within analytical errors suggesting relatively simple, closed-system behavior of the U–Pb age systems, but  $\sim 6\%$  of the grains do show clear evidence of either Pb-loss (defined here as discordance exceeding 10%) or multiple age domains.

We also identified three zircons with textures suggestive of formation in an impact environment. Two grains from sample 15455, Z3 and Z24, are characterized by granular texture recrystallization, with isolated anhedral baddeleyite ( $\text{ZrO}_2$ ) domains within some granules (Fig. 2). Two analyses of Z3 yield concordant ages of  $4331 \pm 3$  and  $4322 \pm 4 \text{ Ma}$  ( $1\sigma$ ) and one analysis of Z24 gives a  $4332 \pm 3 \text{ Ma}$  age ( $1\sigma$ ). A third granular zircon from soil 14259,664 Z24 has a concordant age of  $4195 \pm 7 \text{ Ma}$  ( $1\sigma$ ), however it does not contain regions of decomposed zircon (i.e.  $\text{ZrO}_2$  and  $\text{SiO}_2$ ). Interpretation of these ages is discussed further in Section 5.1.2.

### 4.2. Rare Earth Elements and Ti Temperatures

We collected 102 measurements of REE, Ti, Hf, Th, U, and Fe concentrations for a subset of 90 zircons. We filtered the results to remove analyses that contained inclusions or cracks by inspection of SIMS analysis pits with SEM imaging and by excluding measurements with anomalously high Fe concentration (50 analyses were filtered). Most of the inclusions we observed are associated with annealed fractures and shock features and do not appear primary in nature (examples are shown in Fig. 4). The inclusions also appear dark in BSE images and a fraction for which EBSD analyses were available are amorphous, suggesting most are

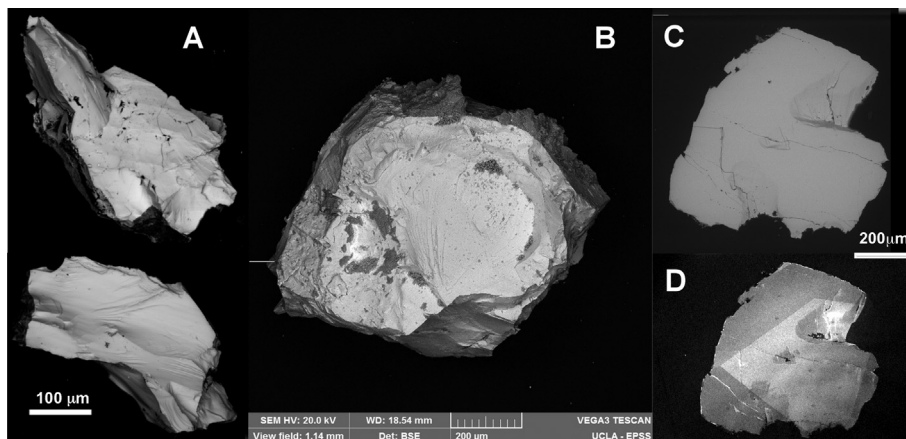


Fig. 1. (A) Secondary electron (SE) images of lunar zircons prior to mounting in epoxy illustrate the fragmented nature observed in the majority of lunar zircons. (B) SE image of 14259,664 Z1 prior to mounting; this is the largest zircon recovered in this study and has a diameter of  $\sim 900 \mu\text{m}$ . SE (C) and cathodoluminescence (CL) (D) images of 14259,664 Z1, taken after mounting and polishing, reveal primary zoning suggesting that it was once part of a larger parent crystal. This zoning implies that zircons  $>1 \text{ mm}$  in size were crystallized on the early Moon, most likely in late stage KREEP magmas.

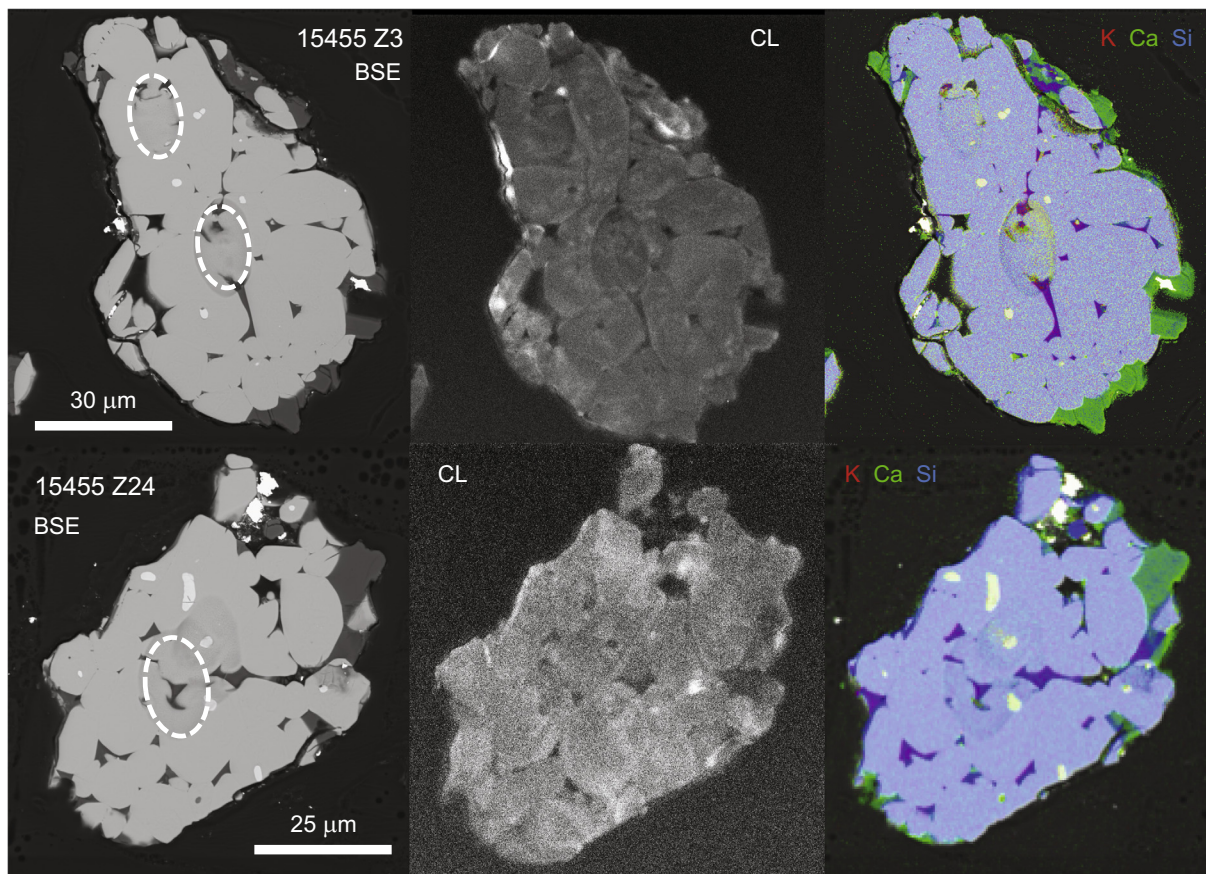


Fig. 2. SEM images of Apollo 15 granular texture zircons. Here we define granular texture as a coherent zircon totally or partially comprised of multiple sub-crystals, that are typically euhedral or subhedral in nature. Both zircons, 15455 Z3 and 15455 Z24, are comprised of multiple large granules with remnant baddeleyite cores that appear bright in the backscatter electron (BSE) and correlate with Si deficiencies in EDS maps. The interstitial material (purple in EDS map) is not the same as the surrounding plagioclase (green in EDS map); it is K-Si-O rich and does not produce an electron backscatter pattern (EBSP) suggesting it is most likely glass. The presence of baddeleyite and interstitial (impact) melt makes these two grains the most likely candidates for impact grown zircons in our sample set. Two SIMS analyses (dashed circles in BSE images) of Z3 have an average  $^{207}\text{Pb}$ – $^{206}\text{Pb}$  age of  $4326 \pm 5 \text{ Ma}$  ( $1\sigma$ ) and one analysis of Z24 yields an age of  $4332 \pm 3 \text{ Ma}$  ( $1\sigma$ ), suggesting formation in an impact event at  $\sim 4.330 \text{ Ga}$ .

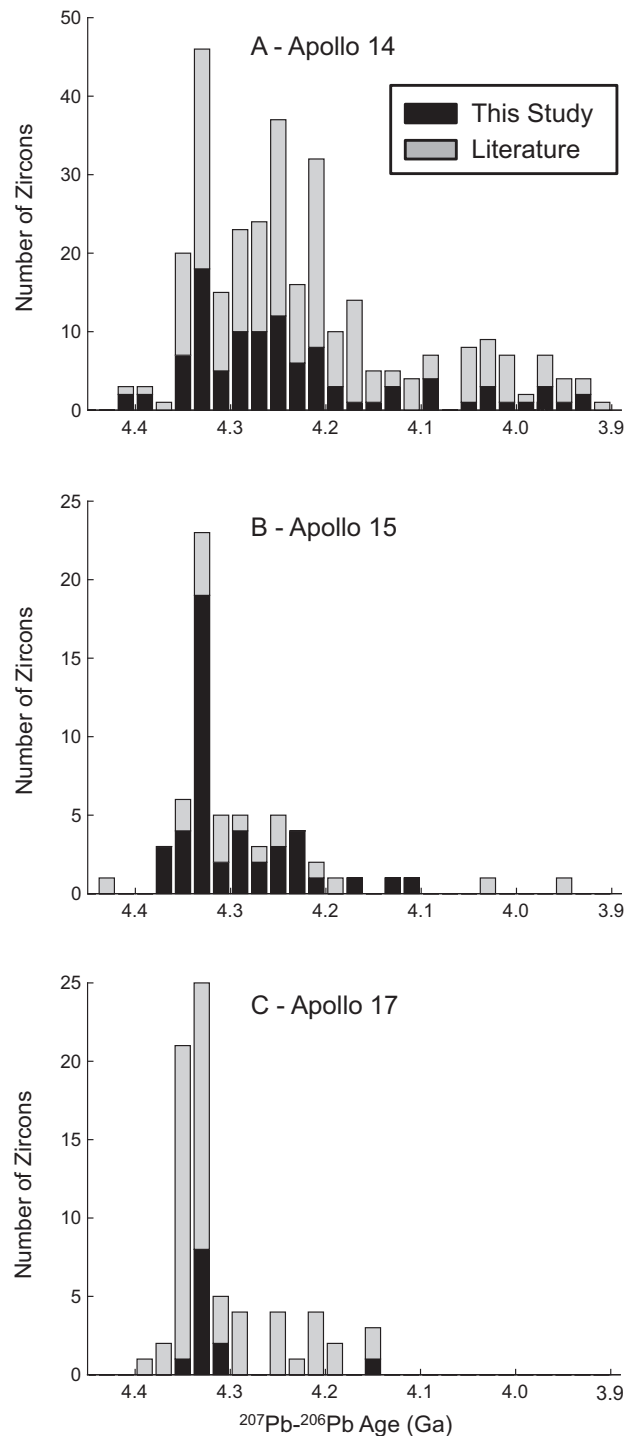


Fig. 3.  $^{207}\text{Pb}$ – $^{206}\text{Pb}$  age histograms for Apollo 14 (307 zircons), 15 (52 zircons) and 17 (76 zircons) zircons (black – this study; grey – literature data; references below), which are considered lower limits on crystallization ages. In the histograms we included only the oldest age for zircons with multiple age analyses and excluded ages of impact grown/recrystallized zircons, which are shown in Fig. 8. Apollo 14 zircons span the full range of ages from 3.9 to just over 4.4 Ga, while all but two zircons from Apollo 15 and 17 are older than 4.1 Ga. The two young Apollo 15 zircons are from highly disturbed grains with evidence of Pb-loss between 1 and 2 Ga, so these data may not be good estimates of crystallization age (Meyer et al., 1996; Grange et al., 2013b). The age distributions for Apollo 15 and 17 are dominated by zircons between 4.30 and 4.35 Ga. This peak is less pronounced in the Apollo 14 data where the majority of zircons are between 4.2 and 4.35 Ga. The observation of primary growth zoning in only those zircons older than 4.2 Ga paired with the distribution of  $^{207}\text{Pb}$ – $^{206}\text{Pb}$  ages suggests that zircon forming KREEP magmatism ceased between 4.2 and 4.1 Ga. (Meyer et al., 1996; Nemchin et al., 2006, 2008; Pidgeon et al., 2007; Taylor et al., 2009b; Grange et al., 2013a, 2013b; Hopkins and Mojzsis, 2015).

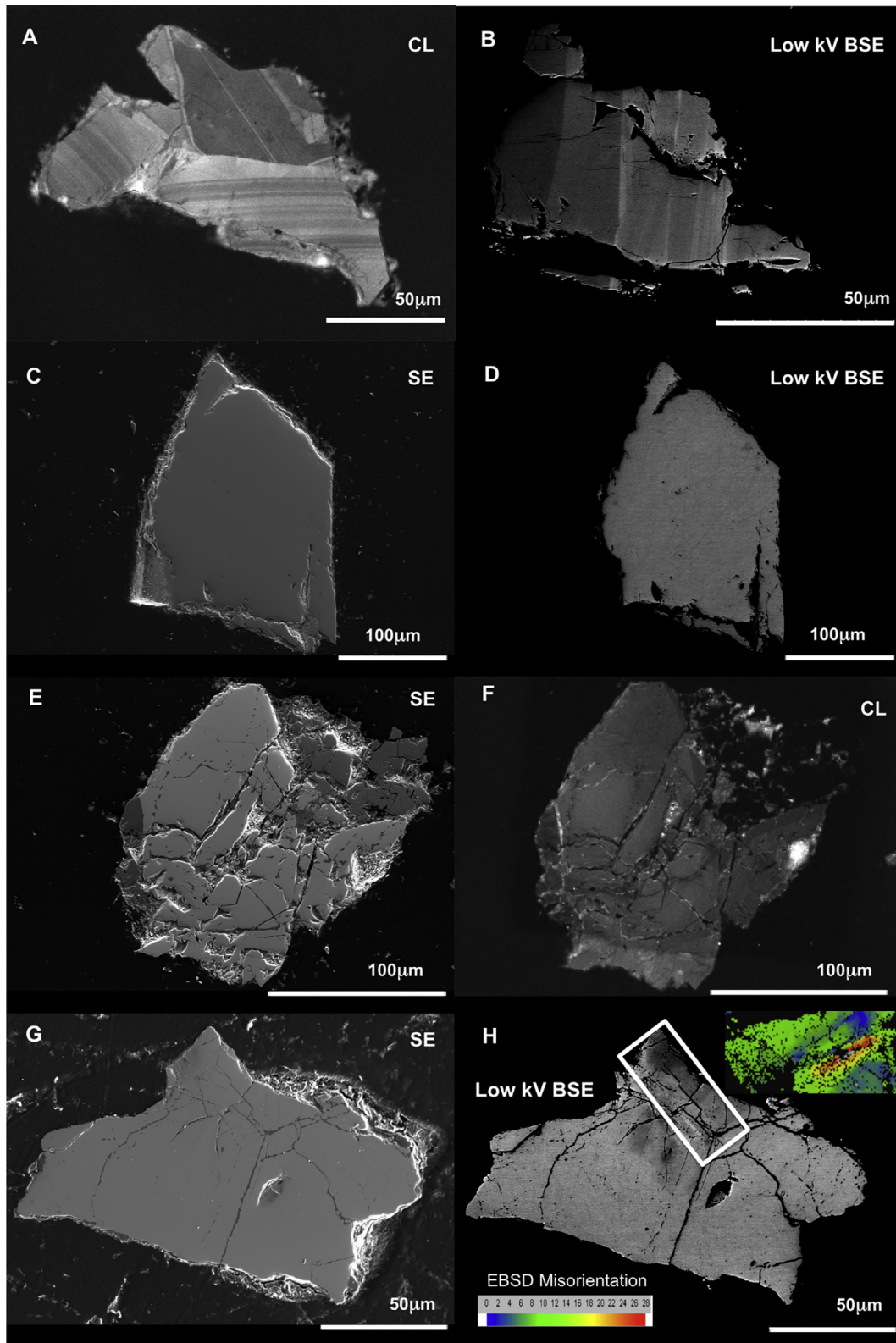


Fig. 4. Examples of primary zoning and secondary impact shock textures observed in lunar zircons. Zircons 14305 Z27 (A) and 14305 Z29 (B) contain well-preserved primary oscillatory and sector growth zoning. SE and Low kV BSE images of zircon 14321 Z14 (C and D) are very homogeneous and show little evidence of shock alteration other than fragmentation. This homogeneity is reflected in seven trace element analyses, however five U–Pb analyses reveal significant discordance (see Fig. 6). 14305 Z30 (E and F) is one of the most shock-fractured and impact melt-infiltrated zircons recovered in this study and illustrates the difficulty of analyzing REEs in some samples with SIMS spot sizes of  $\sim 20\text{--}30\ \mu\text{m}$ . Another highly shocked zircon, 15311, 18 Z6 (G and H), is almost completely amorphous with only the darkest regions of the Low kV BSE image indexing in EBSD analyses. Despite lack of crystallinity and the high degree of strain (up to  $28^\circ$ ) observed in EBSD, this zircon retains  $^{207}\text{Pb}\text{--}^{206}\text{Pb}$  ages between  $4245 \pm 4$  and  $4332 \pm 3$  ( $1\sigma$ ) Ma (see Fig. 7).

impact melt glasses similar to those described in terrestrial impact zircons (e.g. Moser et al., 2011). The remaining pristine lunar zircon analyses can be characterized by one typical REE pattern, which varies in overall REE concentration between grains. All the zircons exhibit a steep positive slope with LREE depletion and large negative Eu anomalies. In addition to the analyses reported herein, we reevaluated the trace element data reported in Taylor et al. (2009a) with the same set of criteria and filtered out 16 of the 37 analyses due to apparent contributions from inclusions. The remaining pristine zircon measurements from Taylor et al. (2009a) are consistent with the same REE pattern reported herein. The CI-chondrite normalized REE patterns for pristine analyses and the unfiltered Taylor et al. (2009a) dataset are shown in Fig. 5. Trace element data for pristine analyses can be found in Appendix A. CI-chondrite values from McDonough and Sun (1995) were used for normalization.

The concentration of Ti in zircon has been shown to be a function of crystallization temperature and the activities ( $a$ ) of  $\text{SiO}_2$  and  $\text{TiO}_2$  in the parent melt (Watson and Harrison, 2005; Ferry and Watson, 2007; Fu et al., 2008), with relatively little to no influence from variations in pressure or oxygen fugacity ( $f_{\text{O}_2}$ ) (Ferriss et al., 2007; Burnham and Berry, 2012). We calculated Ti-in-zircon temperatures following the calibration derived by Ferry and Watson (2007) and new estimates of  $a_{(\text{SiO}_2)}$  and  $a_{(\text{TiO}_2)}$ . The Ti-temperatures range between  $958 \pm 57^\circ$  and  $1321 \pm 100^\circ \text{C}$ , which are bound by the dry granite solidus and the zircon saturation temperature of KREEP rich rocks (see Section 5.2.3 for further discussion of oxide activities and saturation temperatures).

## 5. DISCUSSION

### 5.1. U–Pb and $^{207}\text{Pb}$ – $^{206}\text{Pb}$ ages: what are they dating?

The distinct decay chains of  $^{238}\text{U}$  to  $^{206}\text{Pb}$  and  $^{235}\text{U}$  to  $^{207}\text{Pb}$  provide an important advantage as a chronometer of ancient samples. Following crystallization, if a sample experiences subsequent Pb-loss, both daughter isotopes will be lost with equal probability. If the Pb-loss event is recent, the Pb isotopic ratio remains unchanged allowing for a  $^{207}\text{Pb}$ – $^{206}\text{Pb}$  age to be computed, and the open system behavior is recognized by discordance in the respective  $^{238}\text{U}/^{206}\text{Pb}$  and  $^{235}\text{U}/^{207}\text{Pb}$  ages. In the case of an ancient partial Pb-loss event, however, it can be difficult to recognize discordance in SIMS analyses with relatively large uncertainties in individual  $^{238}\text{U}/^{206}\text{Pb}$  and  $^{235}\text{U}/^{207}\text{Pb}$  ages. The uncertainties in our analyses are limited by the inter-element relative sensitivity factors (average  $1\sigma$  is  $\sim 180$  Ma for  $^{207}\text{Pb}$ – $^{235}\text{U}$  age, and  $\sim 60$  Ma for  $^{206}\text{Pb}$ – $^{238}\text{U}$  age). But even in cases of large errors, the  $^{207}\text{Pb}$ – $^{206}\text{Pb}$  ages can be strictly interpreted as a lower limit on either the igneous age of the sample or the time of last total Pb-loss.

On Earth, Pb-loss in zircon is facilitated by interactions with fluids and metamictization (i.e. structural damage of the crystal lattice induced by alpha particles emitted by U). The latter forms amorphous regions in crystals that provide accelerated pathways for Pb-loss as they are easily infiltrated by fluids (e.g. Mezger and Krogstad, 1997). Despite recent findings of high OH contents in late-crystallizing phases, the lunar crust is dry (e.g. Boyce et al., 2014). Additionally, the majority of lunar zircons have U concentrations below 100 ppm, which is not high

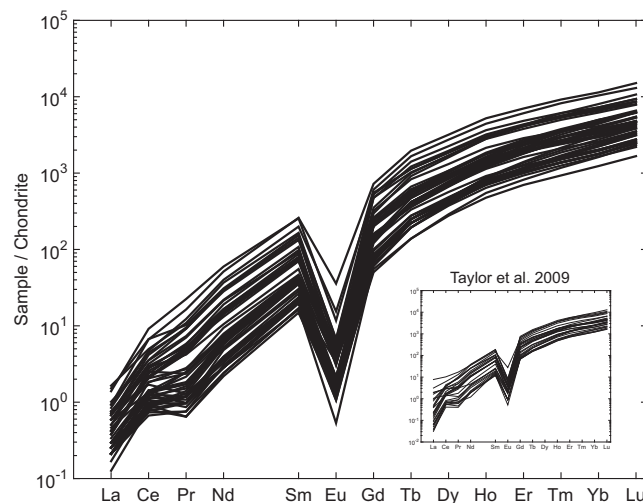


Fig. 5. Chondrite normalized REE patterns for pristine zircon analyses (38 from this study; 21 from Taylor et al. (2009a, 2009b)). All analyses with Fe concentrations  $>400$  ppm or visible sources of contamination were excluded. The zircons can generally be described by one REE pattern with varying total concentrations. The pattern has a steep positive slope resulting from the zircon trace element partition coefficients and a negative Eu anomaly due to removal of plagioclase prior to zircon formation. The figure inset contains all REEs analyses reported from Taylor et al. (2009a, 2009b); zircons with LREE enrichments were found to contain contributions from inclusions and/or surrounding phases. Chondritic values from McDonough and Sun (1995) were used for normalization.

enough to cause appreciable amounts of metamictization, so these two processes are not likely mechanisms for Pb-loss in zircons from the Moon (Wopenka et al., 1996; Garver and Kamp, 2002). This assumption is also supported by the high crystallinity of most zircons observed in EBSD analyses. Impacts are the dominant geologic alteration process on the surface of the Moon and, without the presence of water or high levels of metamictization, impact heating and shock are the most likely sources of U–Pb system disturbances in zircon. Whether lunar zircon ages reflect igneous (i.e., primary) crystallization or later impact alteration event(s) remains controversial, however guidelines for age interpretations have been proposed based on a combination of both lunar and terrestrial shocked grains.

In terrestrial impact structures, zircons that have recrystallized as a result of impact heating or contain structural damage in the form of crystal plastic deformation do show evidence of Pb-loss (post impact hydrothermal alteration can also cause Pb-loss, but this scenario is not applicable to the Moon). In cases of recrystallization, the zircons experience 80–100% Pb-loss with lower Concordia intercepts consistent with the age of the impact responsible for the recrystallization (e.g. Moser et al., 2011). Grange et al. (2013a) observed similar behaviors in lunar zircons and presented guidelines for interpreting lunar zircon U–Pb and  $^{207}\text{Pb}$ – $^{206}\text{Pb}$  ages based on microstructural investigations using SEM and EBSD imaging. They also suggested that the  $^{207}\text{Pb}$ – $^{206}\text{Pb}$  ages of lunar zircons are only fully reset in the cases of zircon growth or recrystallization in an impact setting. Partial Pb-loss was observed in grains wherein post-impact strain caused high degrees of crystal plastic deformation. In these cases of open-system behavior, and in grains with multiple age domains, both the igneous ages and impact ages could be constrained.

### 5.1.1. Age distributions

The distributions of the  $^{207}\text{Pb}$ – $^{206}\text{Pb}$  ages for Apollo 14, 15, and 17 zircons reported herein agree well with previously reported lunar zircon ages (Meyer et al., 1996; Nemchin et al., 2006, 2008; Pidgeon et al., 2007; Taylor et al., 2009b; Grange et al., 2013a, 2013b; Hopkins and Mojzsis, 2015). Nemchin et al. (2008) observed no variation in zircon age distributions among samples within a given Apollo landing site and concluded that it is appropriate to analyze summed, or composite, histograms. We therefore present the age histograms grouped by Apollo mission in Fig. 3.

The age distributions for all three landing sites have a marked peak around  $\sim 4.33$  Ga with relatively few zircons forming before this time. This peak could simply reflect the onset of zircon saturation in residual KREEP magmas, or the  $\sim 4.33$  Ga population could represent a large zircon-forming event related to either LMO crystallization processes (such as mantle overturn) or a large impact basin (such as South Pole Aitken) (e.g. Elkins Tanton et al., 2002; Kring et al., 2015). There is also a notable lack of post-4.1 Ga zircons from Apollo 15 and 17 samples.

We employed a Mann–Whitney U-test to determine if the variations in age distributions between landing sites are statistically significant (Mann and Whitney, 1947). This

test compares the ranked-sums of two data sets to determine if they are sampling the same parent population (the Null hypothesis). Because more than two datasets are being compared, we also applied a Bonferroni correction to account for multiple comparisons (Rice, 1989). This correction states that the probability for individual tests must be less than the desired significance level divided by the number of tests performed. This means if we want to determine that the age distributions are sampling different populations at a significance level of 0.05, then the probability of the Null must be less than 0.017 for each Mann–Whitney U-test. The probabilities that either the Apollo 15 or the Apollo 17 histograms are sampling the same zircon age distribution as Apollo 14 are both  $<0.0003$ , therefore the Apollo 15 and 17 zircon ages are statistically different from those of Apollo 14 (rejecting the Null hypothesis). However, a similar comparison between Apollo 15 and 17 yields a probability of 0.022, which is not below 0.017. These two landing sites could therefore be sampling the same zircon population.

Only  $\sim 10\%$  of the lunar zircons reported herein, and described in literature, are in the  $<4.1$  Ga population observed in Apollo 14. Most of these zircons have small grain sizes ( $<50$   $\mu\text{m}$ ) or exhibit open system behavior either as multiple age domains or discordant U–Pb ages (Figs. 6 and 7). Apollo 12 zircons have also been shown to contain a subset of grains that are  $<4.1$  Ga (Meyer et al., 1996; Zhang et al., 2012). Similar to the Apollo 14 zircons, the younger grains from Zhang et al. (2012) exhibit microstructural textures that have been associated with impact induced Pb disturbance or have small grain sizes. Interestingly, the Apollo 12 and 14 landing sites are geographically close, whereas Apollo 15 and 17 are located on the rims of Imbrium and Serenitatis basins respectively. Apollo 12 and 14 landing sites are also thought to sample Imbrium ejecta, which has an estimated age between 3750 and 3938 Ma based on Rb–Sr, K–Ar, and Sm–Nd of Apollo 14 rocks and U–Pb ages of zircons and phosphates from similar samples (e.g., Deutsch and Stöfler, 1987; Shih et al., 1987; Stadermann et al., 1991; Liu et al., 2012; Merle et al., 2014). Imbrium ejecta is a potential source of the younger,  $<4.1$  Ga zircon population either through disturbance of the U–Pb systems during the impact event or through excavation of younger material that is not sampled by Apollo 15 and 17. A dedicated investigation of the younger zircon population would help in determining the extent of Imbrium influence on these samples. In the following two sections we discuss in more detail both the impact and igneous crystallization ages inferred from the lunar zircons reported herein.

### 5.1.2. Impact ages

The most robust lunar zircon impact ages come from grains belonging to a type of granular zircon texture indicative of post-impact recrystallization. The granular or polycrystalline zircon texture is known to occur in both tectonic and impact settings. Tectonic granular zircon can result from either a replacement reaction of zircon after baddeleyite in metagabbroic rocks (e.g. Davidson and van Breeman, 1988) or high temperature annealing following

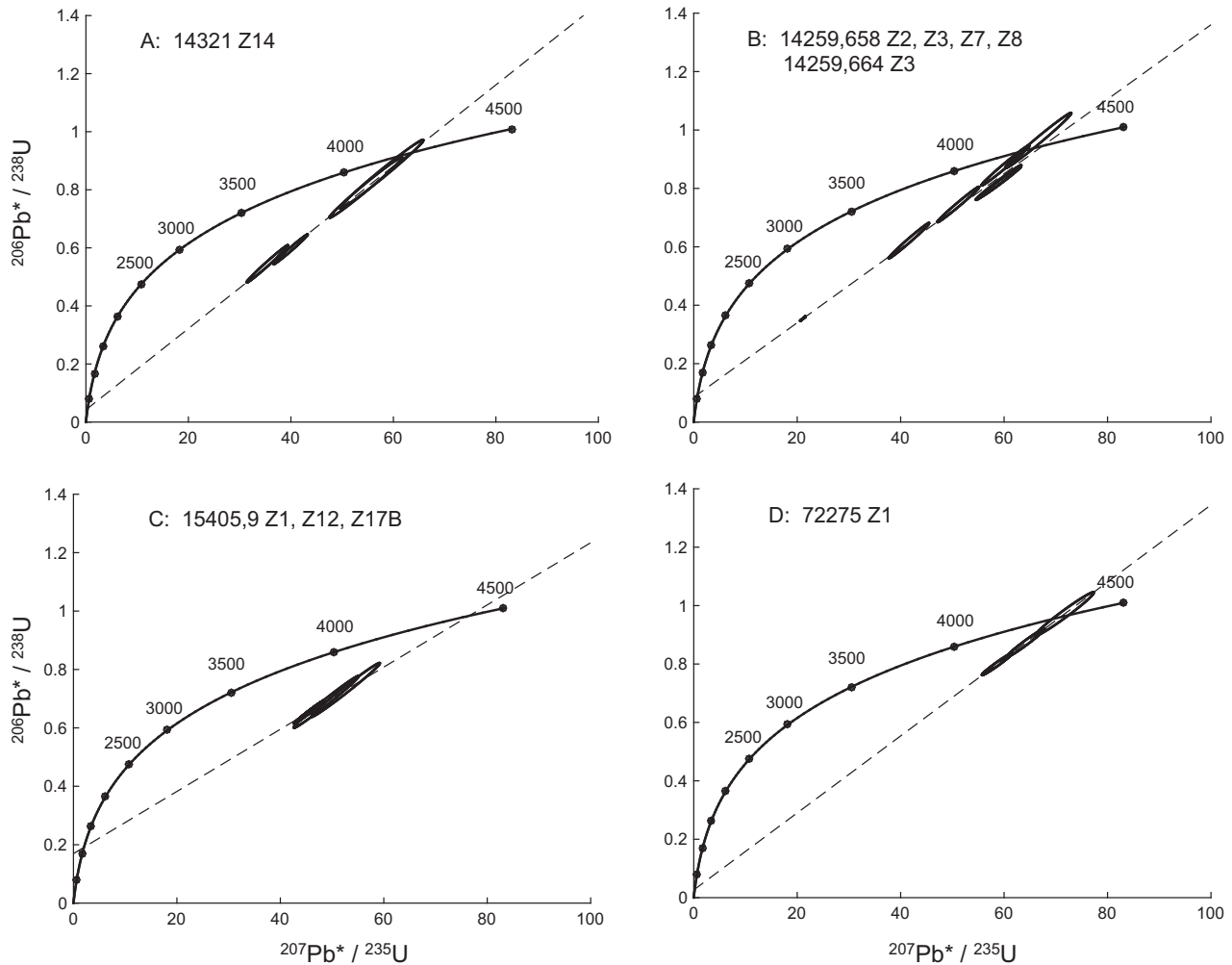


Fig. 6. Concordia diagrams for all zircons that display >10% discordance suggest recent Pb-loss within the last ~1 Ga (data plotted with  $1\sigma$  uncertainties). (A) Four analyses of 14321 Z14 (Fig. 4c,d) suggest recent Pb-loss at  $288 \pm 228$  ( $1\sigma$ ) Ma. Apollo 14 soil zircons (B) and zircon 72275 Z1 (D) follow similar trends with lower Concordia intercepts of  $584 \pm 179$  ( $1\sigma$ ) Ma and  $245 \pm 310$  ( $1\sigma$ ) Ma, respectively. (C) Four analyses of 15405,9 zircons also suggest recent Pb-loss, however the lower intercept is not well constrained due to small spread in U–Pb ratios. Ages and errors were calculated following Ludwig (1980).

zircon deformation in shear zones (e.g. Kovaleva et al., 2014). In both cases the average granule is  $\geq 10 \mu\text{m}$ , has relatively low angular misorientation and exhibits relict primary CL zoning (Cavosie et al., 2015). In impact settings two end-members of granular zircon are observed with coarse ( $\geq 10 \mu\text{m}$ ) or fine ( $\sim 1 \mu\text{m}$ ) granule sizes. The latter are unique to ejecta deposits (e.g. Krogh et al., 1993) and suevitic and tektite glasses (Kleinmann, 1969) where grains are exposed to temperatures above  $1673 \text{ }^\circ\text{C}$ , at which zircon decomposes to its constituent oxides  $\text{ZrO}_2$  and  $\text{SiO}_2$  (Kaiser et al., 2008). The coarse variety of granular impact zircons have so far been found as zircon xenocrysts in mafic impact melt as well as crater floor rocks in large  $\sim 250 \text{ km}$  diameter impact structures in sites proximal to impact melt bodies (Moser, 1997; Moser et al., 2011). Intermediate (up to  $\sim 2 \mu\text{m}$ ) granular zircon has been reported from fine-grained crystalline impact melt from the center of the Australian Acraman impact with the distinctive feature of  $\text{ZrO}_2$

inclusions resulting from shock stage IV ( $>65 \text{ GPa}$ ,  $>1500 \text{ }^\circ\text{C}$ ) (Schmieder et al., 2015). Coarse granules in these settings exhibit internal, concentric CL zoning (Moser et al., 2011; Cavosie et al., 2015). The Apollo 15 granular zircons exhibit the characteristics of grains from the high pressure and ultrahigh temperature (UHT) crater floor environment such as the concentric CL zoning of granules and micron-scale domains of baddeleyite ( $\text{ZrO}_2$ ) (Fig. 2). They also contain alkali aluminosilicate material infilling the interstices of the neoblasts (Fig. 2) that does not diffract and is similar to the impact melt glass seen along curved and planar shock features in our other Apollo grains and UHT-shocked Vredefort grains (Moser et al., 2011).

The U–Pb analyses of the two granular zircons from 15455 (Z3 and Z24) have a slight apparent reverse discordance due to the  $\text{ZrO}_2$  cores in some granules (affecting calibration of U/Pb relative sensitivity factors), however their  $^{207}\text{Pb}$ – $^{206}\text{Pb}$  ages may suggest an impact event at

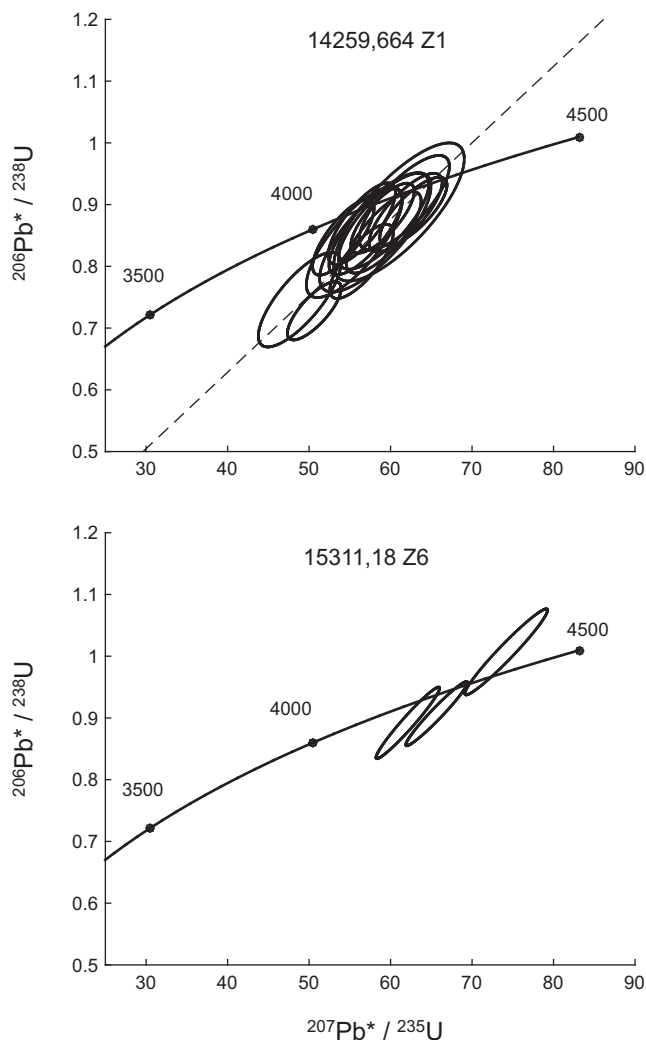


Fig. 7. Concordia diagrams for two lunar zircons with multiple  $^{207}\text{Pb}$ – $^{206}\text{Pb}$  domains (data plotted with  $1\sigma$  uncertainties). (A) Zircon 14259,664 Z1 is the largest zircon recovered in this study and exhibits nearly concordant behavior with  $^{207}\text{Pb}$ – $^{206}\text{Pb}$  ages ranging between 4075 and 4312 Ma. Some analyses of this grain also appears to be affected by the recent Pb-loss event observed in other 14259 soil zircons, which could explain some of the spread in apparent ages. (B) Three analyses of highly shocked grain 15311,18 Z6 (Fig. 4G,H) yield concordant ages ranging from 4245 to 4332 Ma.

~4.330 Ga. This age is similar to that of a skeletal zircon from sample 73217,52, which has a weighted average  $^{207}\text{Pb}$ – $^{206}\text{Pb}$  age of  $4333 \pm 5$  Ma (Nemchin et al., 2008; Grange et al., 2009: Zircon type-2). Grange et al. (2013b) reported another grain consisting of a mixture of granular texture zircon and baddeleyite from 15405,145 (grain m3). However, U–Pb analyses of this grain yield ages between  $2053 \pm 14$  and  $4185 \pm 3$  Ma and define a discordia with a lower intercept of  $1938 \pm 96$  Ma, indicating a significantly younger impact event than our baddeleyite-bearing grains. Grange et al. (2013a) also reported a skeletal zircon from related 73215 that shows a spread of ages between 4305 and 4378 Ma. They suggested that the zircon formed in an initial impact at ~4.38 Ga and underwent later Pb-loss at 4.31 Ga. Despite the age similarities between the skeletal zircons and the 15455 grains, it is difficult to tell if they formed as the result of one impact or separate events.

It is interesting to note that the timing of the impact events in the 15455 and 73215 samples coincides with the ~4.33 Ga peak seen in the age distributions of all three landing sites, and the majority of the zircons in this peak show no microstructural evidence to support impact resetting. It is unclear if this coincidence suggests an impact trigger for a large, zircon-forming event or if it stems from the paucity of pre-4.35 Ga zircons and the necessity to have pre-existing zircon grains to record impact recrystallization textures such as granularization or decomposition to baddeleyite.

We analyzed a third granular grain 14259,664 Z24 that does not contain baddeleyite cores, but does have large granules ( $>20 \mu\text{m}$ ) and lacks relict CL zoning (see supplementary material for SEM imaging of this zircon). This grain does not resemble tectonically recrystallized zircons, and its texture is most likely impact related. Two analyses

on two separate granules of this zircon yield a concordant average age of  $4195 \pm 7$  Ma ( $1\sigma$ ). Similar impact ages have previously been suggested based on zircon and accessory phase U–Pb analyses. Smith et al. (1986), Pidgeon et al. (2007) and Bellucci et al. (2016) determined an  $4184 \pm 7$  Ma ( $1\sigma$ ) age for recrystallized domains in a 73235 zircon aggregate (also known as the pomegranate zircon), which they suggest formed due to a distant impact event at this time. It is also worth noting the similarity between these ages and the 4.2 Ga basin-forming age proposed based on U–Pb ages of zirconolite and apatite grains in Apollo sample 67955 (Norman and Nemchin, 2014). The response of the U–Pb system to impact environments may not be identical for zircon and other accessory phases, so it is difficult to determine if these events are related.

In addition to textural analyses, evidence of age resetting can be identified in grains that exhibit open system behavior. In these cases, bounds can be placed on the crystallization and impact ages, however precise ages are hard to determine due to difficulty in constraining ancient Pb-loss. Only 6% of the grains we analyzed exhibit discordant behavior or contain multiple age domains suggesting that the majority of lunar zircon  $^{207}\text{Pb}$ – $^{206}\text{Pb}$  ages are not disturbed (Fig. 6).

Seven Apollo 14 zircons (14259,658 Z2, Z3, Z7, Z8; 14259,664 Z1, Z3; 14321 Z14), three Apollo 15 (15405,9 Z1, Z12, Z17B) and one Apollo 17 zircon (72275 Z1) show U–Pb discordance greater than 10%. The discordant Apollo 14 grains appear to have experienced a recent Pb-loss event. Five analyses of the individual breccia zircon 14321 Z14 define a discordia line with a lower intercept of  $288 \pm 228$  ( $1\sigma$ ) Ma (Fig. 6A). The 14259 soil zircons also follow a similar trend with a Pb-loss event at  $584 \pm 179$  ( $1\sigma$ ) Ma (Fig. 6B). This behavior has also been noted in U–Pb analyses of agglutinates from the same soil sample (Church et al., 1976). The analyses of Apollo 15 zircons show recent Pb-loss within the last  $\sim 1$  Ga, however the Concordia intercepts are difficult to constrain since there is very little spread in the data (Fig. 6C). Three analyses of 72275 Z1 define a discordia with a lower intercept of  $245 \pm 310$  ( $1\sigma$ ) Ma and an upper intercept of  $4347 \pm 40$  ( $1\sigma$ ) (Fig. 6D). It is interesting to note that all the discordant zircons appear to be affected by a recent Pb-loss event within the last  $\sim 900$  Myr (based on the lower Concordia intercepts assuming  $2\sigma$  errors). This is an unexpected observation since most of the zircons crystallized prior to the proposed lunar cataclysm and show no evidence of Pb-loss resulting from hypothesized  $\sim 3.9$  Ga basin-forming events. However, it is plausible that moderately sized impacts could produce localized thermal and shock regimes capable of inducing open system behavior. The volumes of affected material would be relatively small in this scenario, which, along with sample biases, may explain the relative scarcity of discordant grains. Ejecta from craters Tycho ( $109 \pm 4$  Myr) and Copernicus ( $800 \pm 15$  Myr) have been identified in both Apollo 12 and 17 samples and are potential sources of the recent Pb-loss event(s) observed in our data (Eberhardt et al., 1973; Arvidson et al., 1976; Lucchitta, 1977; Bogard et al., 1994; Stöffler and Ryder, 2001).

We collected multi-spot analyses for 26 zircons, and of these only four show variations in the concordant ages outside of the  $2\sigma$  errors. Most notable are grains 15311,18 Z6 and 14259,664 Z1. EBSD analyses of 15311,18 Z6 reveal that this grain is almost completely amorphous and cross-cut by a complex pattern of curvilinear features (see Fig. 4G and H). Despite being almost fully amorphous, it retains relatively old  $^{207}\text{Pb}$ – $^{206}\text{Pb}$  ages ranging from  $4245 \pm 4$  to  $4332 \pm 3$  ( $1\sigma$ ) Ma. These data suggest a lower limit on crystallization of 4.33 Ga and an upper age limit of Pb-loss of 4.25 Ga (Fig. 7 bottom). The second grain, 14259,664 Z1, is  $\sim 900$   $\mu\text{m}$  in diameter (the largest zircon we have analyzed to date) and, based on CL zonation (Fig. 1D), it appears to be a fragment of an even larger parent zircon. The  $^{207}\text{Pb}$ – $^{206}\text{Pb}$  ages of this zircon span from  $4075 \pm 8$  to  $4313 \pm 8$  ( $1\sigma$ ) with discordance in only a few analyses (Fig. 7 top). The younger ages appear to be associated with cracks that may have served as pathways for increased Pb-loss during a thermal event. The most discordant analyses result from recent Pb-loss with a similar age as the disturbance observed in the other 14259 soil zircons. However, with the precision of SIMS U–Pb analyses, it is difficult to determine if the spread in concordant ages is a result of recent Pb-loss or a more ancient event, the upper age limit of which is 4.08 Ga. Here we stress again that multiple age domains and discordance can only be used to place limits on impact ages, and therefore impact grown or recrystallized zircons yield the most robust determination of impact ages.

In addition to the samples discussed above, previous studies have identified recrystallized and/or impact derived zircons that yield ages around  $\sim 3.9$  Ga and  $\sim 4.1$  Ga. Grange et al. (2013a) identified a zircon in 73235 (“Tiger” zircon) with recrystallized domains that have an age of  $4106 \pm 18$  Ma. Grange et al. (2009) reported a  $^{207}\text{Pb}$ – $^{206}\text{Pb}$  age of  $3929 \pm 10$  Ma for a granular texture zircon (type-3) reaction rim surrounding a baddeleyite grain in sample 73217. A similar age of  $3927 \pm 8$  Ma was determined for a poikilitic zircon from 14311,20 (ts3-24) by Hopkins and Mojzsis (2015) (some regions of this grain appear similar to the granular texture zircons discussed herein). A second poikilitic/granular zircon from this sample (ts2-3) has a slightly older age of  $3954 \pm 13$  Ma. An even younger event was suggested by the 15405 zircons from Meyer et al. (1996) and Grange et al. (2013b), which define a line with a lower concordia intercepts of  $1320 \pm 250$  Ma and  $1733 \pm 130$  Ma, respectively.

Although Apollo 14, 15, and 17 samples are the main focus of this article, we include Apollo 12 and lunar meteorites in our enumeration of lunar zircon impact ages to better develop an understanding of the global lunar impact flux. Interstitial and poikilitic/sieved texture zircons contained within impact melt breccias from Apollo 12 samples and lunar meteorite SaU 169 have average ages of  $3914 \pm 7$  Ma and  $3920 \pm 13$  Ma respectively (Liu et al., 2012). The ages of these grains have been used to argue for an impact event at  $\sim 3.9$  Ga. A 4.2 Ga impact event was also suggested by Zhang et al. (2012) based on a peak in the  $^{207}\text{Pb}$ – $^{206}\text{Pb}$  ages of Apollo 12 zircons, however no textural evidence for this interpretation is given.

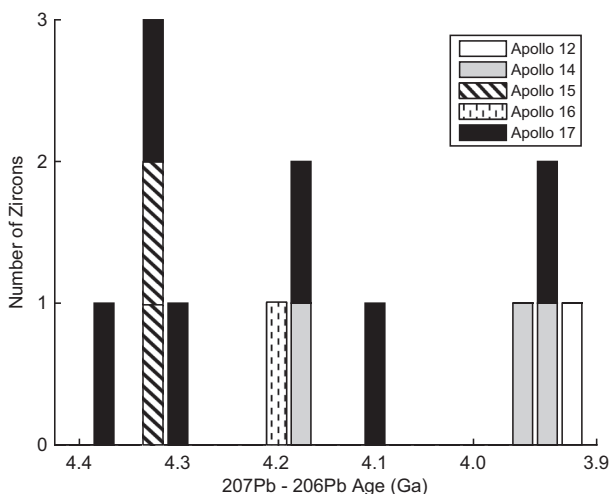


Fig. 8. Age histogram for impact grown or recrystallized lunar zircon and zirconolite grains. These  $^{207}\text{Pb}$ – $^{206}\text{Pb}$  ages suggest that large impact events occurred at least as often as every 100 Myr on the Moon prior to the hypothesized Late Heavy Bombardment era. (Smith et al., 1986; Pidgeon et al., 2007; Nemchin et al., 2008; Grange et al., 2009; Liu et al., 2012; Grange et al., 2013a; Norman and Nemchin, 2014; Hopkins and Mojzsis, 2015; Bellucci et al., 2016). Samples 15455 Z3 and Z24 from this study are included in this diagram and have  $^{207}\text{Pb}$ – $^{206}\text{Pb}$  ages of  $\sim 4.33$  Ga.

A histogram of  $^{207}\text{Pb}$ – $^{206}\text{Pb}$  ages of the lunar zircons exhibiting impact growth textures discussed above is presented in Fig. 8. These zircon ages provide evidence for large impacts, possibly basin forming events, occurring at least as often as every  $\sim 100$  Myr after the initiation of zircon formation around 4.4 Ga, until  $\sim 3.9$  Ga. It is difficult to use the abundance of impact grown or recrystallized zircons to constrain the absolute flux of impacts due to factors such as preservation of fragile zircons during sample preparation. However, separation techniques should not preferentially favor zircons of a particular age, so the wide spread of impact ages may suggest a more constant large impact flux on the early Moon than previously thought (Fig. 8 contains 13 ages, most of which are single zircon ages). A similar conclusion has been put forth by previous studies, however in some cases the distribution of igneous crystallization ages of lunar zircons was used to infer ages of large impacts (e.g. Norman and Nemchin, 2014; Hopkins and Mojzsis, 2015). Without textural evidence of impact alteration/growth or ancient Pb-loss, it is difficult to associate these episodes of zircon formation with basin forming events, although further investigation into similarities between the impact and crystallization ages is needed. Interpretations of the igneous crystallization ages of lunar zircons are discussed further in the following section.

### 5.1.3. Igneous crystallization ages

While zircons with impact modification textures or open system behavior are useful in constraining the ages of impact events, they comprise only a small percentage of the grains we analyzed. For the majority of the zircons reported herein, we find no textural evidence of recrystallization or deformation consistent with measurable

Pb-loss, and their U–Pb ages are concordant within error. We therefore interpret the  $^{207}\text{Pb}$ – $^{206}\text{Pb}$  ages of these zircons as lower limits on igneous crystallization ages. Even in the cases of open system behavior discussed above, the oldest age or Concordia intercept can still be interpreted as a limit on the crystallization age.

All of the lunar zircons we analyzed are fragments of much larger zircons, and they range in size from  $\sim 20$  to  $900\ \mu\text{m}$ . As previously mentioned, primary igneous growth zoning, seen in CL images, suggests that some of these fragments came from zircon crystals larger than a millimeter in length. Zircons grown in terrestrial impact structures tend to be only a few  $10\ \text{s}$  to  $100\ \mu\text{m}$  in length, which is much smaller than the original, parent lunar zircons (e.g. Moser et al., 2011; Wielicki et al., 2012). A magma that is highly enriched in zirconium is necessary to produce millimeter-sized zircons, and KREEP magmatism is the most likely source for such highly enriched parent melts on the Moon. The crystallization ages of lunar zircons have therefore been used to infer the duration of KREEP magmatism (e.g. Meyer et al., 1989, 1996).

Inspection of the age distributions in Fig. 3 reveals that 90% of all zircons are older than 4.1 Ga, and  $>90\%$  of Apollo 15 and 17 grains are older than 4.2 Ga. In the recent study of Apollo 14 zircons by Hopkins and Mojzsis (2015), igneous growth zoning was predominantly identified in the oldest ( $\sim 4.33$  Ga) zircons, and the ages of these zircons were interpreted as primary crystallization ages. Similarly, microstructural analyses of the samples in the present study reveal that primary igneous zonation is seen only in zircons older than  $\sim 4.2$  Ga (examples of primary zoning are shown in Fig. 4). Paired with the age distributions, this observation suggests zircon producing magmatism predominantly ceased by 4.1–4.2 Ga. Note that if the peaks in the zircon age distributions resulted from impact induced magmatic activity, the relatively small amount of ages at 3.9 Ga and the lack of this signature across Apollo landing sites is not consistent with the a hypothesized global lunar cataclysm at this time. Higher spatial resolution age investigations of this young population of zircons would help determine the role impacts played in their formation and if subsequent Pb-loss is affecting their apparent  $^{207}\text{Pb}$ – $^{206}\text{Pb}$  ages.

If zircons formed in KREEP-rich magmas, then the maximum duration of KREEP magmatism was  $\sim 200$ – $300$  Myr, which is shorter than  $\sim 500$  Myr interval previously proposed based on the full range of zircon  $^{207}\text{Pb}$ – $^{206}\text{Pb}$  ages (Meyer et al., 1989, 1996). A shorter duration of KREEP magmatism was also suggested by Zhang et al. (2012) based on the distribution of Apollo 12 zircon ages. Whether the lunar zircons are forming in a single KREEP reservoir or in multiple enriched parent magma cannot be determined by age alone, but paired trace element analyses can give more insight into the nature of early KREEP magmatism.

## 5.2. Trace elements

Zircons incorporate ppm to wt% concentration levels of trace elements such as U, Th, Hf, REEs, and Ti (Appendix A). The absolute and relative abundances of these elements

have been used to infer aspects of zircon provenance, such as magma compositions, temperature, and oxidation state (Belousova et al., 2002; Watson and Harrison, 2005; Schmitt and Zack, 2012; Trail et al., 2012). The CI-chondrite normalized REE patterns for terrestrial igneous zircons are typically characterized by steep slope from LREE to HREE, a positive Ce-anomaly, and a negative Eu-anomaly; the two anomalies suggest oxidizing conditions and plagioclase fractionation prior to zircon formation respectively (e.g. Hoskin and Schaltegger, 2003; Grimes et al., 2007; Bell and Harrison, 2013). The terrestrial zircon REE abundances range from 10s to 1000s ppm, with zircons from crustal rocks having higher concentrations than zircons from mantle rocks (Hoskin and Ireland, 2000; Belousova et al., 2002; Hoskin and Schaltegger, 2003). Terrestrial impact grown zircons have been shown to retain REEs signatures similar to target rock zircons (Wielicki et al., 2012), making it difficult to identify zircons with impact origin by using REE analysis alone.

Nemchin et al. (2010) reported trace element analyses of 15 lunar zircons and identified four groups based on their REE patterns. They defined both Type 1 and 2 patterns as characterized by a positive slope from La to Lu and negative Eu anomalies, but with total REE concentration being higher in Type 2. Type 3 is differentiated by elevated LREE concentrations, and the one zircon characterized as Type 4 has a positive Ce anomaly. Hopkins and Mojzsis (2015) measured trace elements of 105 zircons in breccia 14311 and noted similar variations in the LREE concentrations. We have analyzed REE concentrations in 90 zircons and reevaluated the 34 zircon analyses from Taylor et al. (2009a, 2009b). Unlike previous work, our analyses of pristine zircon are characterized by a single REE pattern once data are filtered to exclude contributions from inclusions and other features hosting trace element contaminants.

### 5.2.1. Identifying contributions from inclusions

The LREE concentrations in zircon are up to four orders of magnitude lower than those of the HREEs, so they are much more easily affected by trace amounts of contamination (Hinton and Upton, 1991). The higher resolution SEM imaging used in this study, compared to previously published lunar zircon images, revealed that more than half of the lunar zircons we analyzed had potential sources of REE contamination exposed on the surface. These features include impact melt inclusions, cracks, annealed curvilinear features, or regions of trace element exchange between zircon and impact melt (visible in CL). Additionally, inspection of these samples under optical transmission microscopy revealed many grains have subsurface inclusions that could potentially be excavated during SIMS analyses. All of these microstructures can include materials with vastly different trace element concentrations than the host zircon. We therefore discarded all analyses where SIMS spots visibly overlapped these potential sources of contamination.

We also used iron concentration to monitor for inclusions and contaminants in SIMS analyses. Iron is incompatible in the zircon structure; Hoskin and Schaltegger

(2003) determined that primary igneous zircons incorporate at most a few hundred ppm Fe. We chose a threshold Fe concentration of 400 ppm because this is the average lunar zircon Fe concentration reported in Wopenka et al. (1996) and is similar to the highest Fe concentrations found in Hadean Jack Hills zircons, which are of similar ages as the lunar samples. Additionally, zircons in our sample set with anomalously high Ti concentrations also contained elevated Fe concentrations. This correlation was previously noted by Hopkins and Mojzsis (2015) and used to filter Ti analyses of Apollo 14 zircons. We discarded approximately half of our trace element analyses due to visibly identifiable sources of contamination and/or Fe concentrations above ~400 ppm.

After filtering our analyses according to these criteria, all measurements with anomalously high LREE concentrations and positive Ce anomalies (Type 3 and 4 from Nemchin et al., 2010) vanished. To investigate further, we conducted a simple mixing model to assess the relationship between the moderate LREE enrichments, similar to Type 3 zircons from Nemchin et al. (2010), and the non-pristine zircon analyses within our data set. For the model we chose two end-member REE analyses: the least pristine zircon analysis (highest contribution from inclusions and surrounding phases) that had Fe and Ti concentrations of ~4 wt% and ~4500 ppm respectively (15405,9 Z12), and the visibly pristine analysis of 14305 Z25 (Fig. 9@ 1). We were able to reproduce the LREE enrichment observed in a second analysis of 14305 Z25 (Fig. 9 @2) containing impact melt glass inclusions with a mixture containing 7% of the high Fe component and 93% of the pristine 14305 Z25 @1. We conducted this experiment with a range of end member analyses and found that all the LREE enrichments can be explained by similar mixtures of pristine and non-pristine material. The results of the models suggest that small amounts of impact melt glass can readily produce the variations in trace element patterns observed and that a large percentage of lunar zircon REE data is contaminated and should not be interpreted in terms of zircon provenance. Additionally, monitoring Fe concentrations and high resolution SEM imaging may be a systematic way to filter lunar zircon trace element data.

After the removal of the analyses containing trace element contaminants, the lunar zircons can be characterized by one REE pattern with varying levels of total REE concentration, which span the full range between Type 1 and Type 2 zircons proposed by Nemchin et al. (2010) (Fig. 5). The negative Eu anomaly seen in all samples is consistent with the zircons forming from a KREEP reservoir after appreciable amounts of plagioclase had been removed to the flotation crust, and the absence of large Ce anomalies supports the conclusion that the lunar grains formed in reducing magmas (Trail et al., 2012). Some of the data may appear to have small positive Ce anomalies, however, in over half of the samples, the Ce and La concentrations are approaching the detection limits of our analyses therefore identifying Ce anomalies is problematic. The similarity of the lunar zircon REE patterns makes it difficult to use the patterns alone to identify zircons of different provenance.

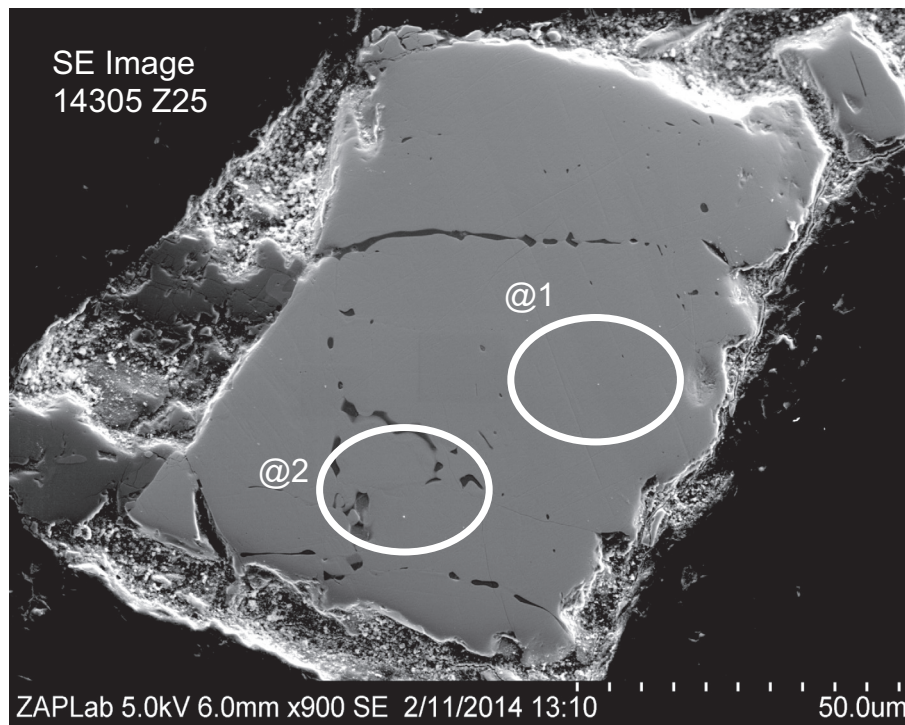
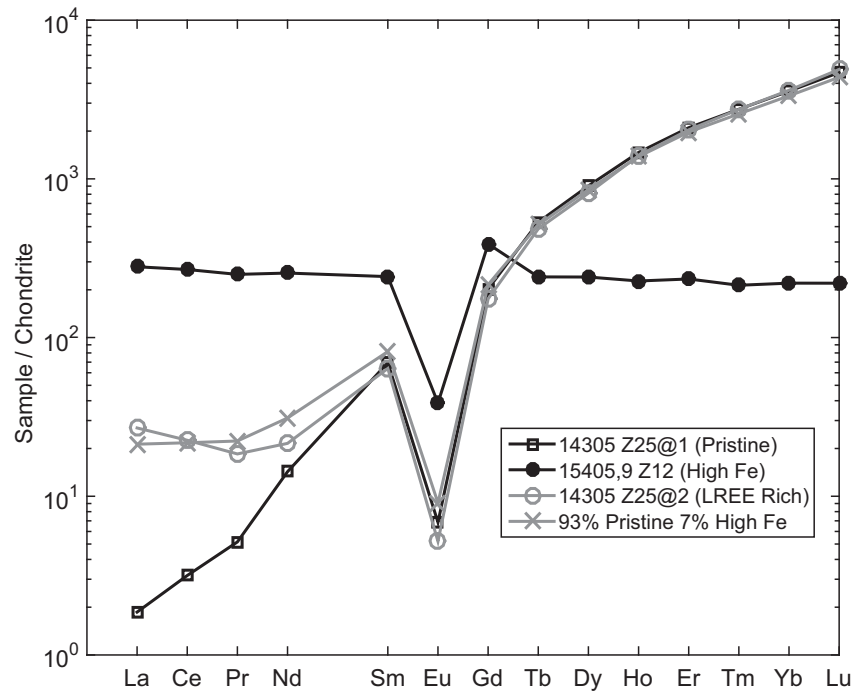


Fig. 9. Linear REE mixing model illustrating the effects of inclusions in SIMS analysis spots. Two analyses of zircon 14305 Z25 exhibit different LREE concentrations and varying amounts of impact melt identified in SE image. The LREE enrichment observed in spot @2 (grey circles) can be reproduced by a mixture of 93% of spot @1 REEs (visibly pristine) and 7% of 15405,9 Z12 (zircon with the highest Fe concentration in this dataset; 4 wt% Fe) (grey Xs). Analyses with identified inclusions or Fe concentrations >400 ppm were therefore not used in characterizing lunar zircon REE patterns (see [Appendix A](#)).

### 5.2.2. Igneous crystallization trends

Lunar zircons are thought to have formed in late stage enriched melts resulting from extensive fractional crystallization of the LMO. [Claiborne et al. \(2010\)](#) showed that

zircons from the Spirit Mountain Batholith, Nevada, record trace element variations indicative of igneous fractional crystallization of parent magmas. As fractional crystallization progresses, Hf becomes increasingly

concentrated in the melt due to its incompatible nature in most minerals. The Hf concentration can therefore be used as a proxy for degree of crystallization within a given magma body. If all the lunar zircons formed from the same original residual magma, one might expect a correlation between the Hf concentration and the  $^{207}\text{Pb}$ – $^{206}\text{Pb}$  crystallization age, but the lunar zircons do not show this correlation. Even among the oldest group of the lunar zircons, >4300 Ma, there is no apparent increase in Hf concentration with progressive crystallization (i.e., a decrease in age). The lack of correlation suggests that either there were multiple parent magmas producing zircons by fractional crystallization or that the zircons are recording conditions in their local environment. It is also possible that the  $^{207}\text{Pb}$ – $^{206}\text{Pb}$  ages have been reset by subsequent impacts that did not simultaneously affect the trace element concentrations. This scenario is feasible because even at 1000 °C, the diffusion coefficients for the REEs are between 4 and 300 times lower than that of Pb (Cherniak et al., 1997; Cherniak and Watson, 2000) as is borne out by shocked terrestrial zircons that experience 80% Pb loss without affecting primary REE zoning (Moser et al., 2011). However, our results do not suggest significant impact related Pb-loss in the lunar zircon population. The trace element data therefore do not support a single KREEP source, although, higher precision U–Pb analyses are needed before the alternative hypothesis can be ruled out.

### 5.2.3. Crystallization temperatures and zircon saturation

As previously mentioned, the partitioning of Ti into zircon is a function of temperature and the activities ( $a$ ) of  $\text{TiO}_2$  and  $\text{SiO}_2$  in the parent melt (Watson and Harrison, 2005). Since almost all lunar zircons are detrital, except for a few found in lithic clasts or exhibiting impact growth textures, the compositions of their parent magmas are unknown. Previous authors have assumed equal values of  $a_{\text{SiO}_2}$  and  $a_{\text{TiO}_2}$ , which may not be appropriate for KREEPY magmas, and they report Ti-in-zircon temperatures for some zircons that extend to subsolidus temperatures (Taylor et al., 2009a, 2009b; Valley et al., 2014; Hopkins and Mojzsis, 2015). In some instances, slightly hydrated late stage KREEPY magmas have been invoked to explain the low temperature zircons, however, this is inconsistent with both the reducing conditions on the Moon and the lack of a Ce-anomaly in the zircon REE data.

Even though we cannot directly measure the  $a_{\text{TiO}_2}$  and  $a_{\text{SiO}_2}$ , we can still determine reasonable values based on estimates of KREEP parent melt compositions. We used the MELTS program to calculate temperatures, activities, and final mineral assemblages for four initial compositions (Ghiorso and Sack, 1995; Asimow and Ghiorso, 1998): (1) estimated composition of urKREEP, or the KREEP parent (Warren and Wasson, 1979), (2) 15405 KREEP basalt granite (Ryder, 1976), (3) 15405 quartz monzodiorite (Taylor et al., 1980), and (4) 70215 high-Ti basalt (LSPET, 1973). The first three are our best estimate of the KREEP parent magma compositions, and the latter was investigated to determine how higher Ti concentrations affect  $a_{\text{TiO}_2}$ . Each MELTS run assumed the following conditions: fractional crystallization,  $P = 0.540$  kbar, initial  $\log f_{\text{O}_2} = \text{IW}-1$

(Ghiorso and Sack, 1995; Wadhwa, 2008), and prohibition of spinel formation. The last parameter was necessary because starting compositions were for samples with little to no spinel, and crystallization of ulvospinel could influence the  $a_{\text{TiO}_2}$ . The MELTS calculated starting temperatures ranged from 1145 to 1324 °C. Zircon is not an optional mineral precipitate in MELTS, however we tracked zircon saturation by assuming that the amount of zirconium stayed constant throughout the MELTS run (i.e. zirconium was not incorporated into crystallizing mineral phases). Zircon saturation was reached for all starting compositions after between  $\sim 1\%$  (QMD 15405 and KREEP) to 86% crystallization (High Ti Basalt).

The  $a_{\text{SiO}_2}$  for all four compositions varied between 0.5 and 0.7 for the duration of the MELTS models; there is a slight increase in silica activity with decreasing temperature and increasing degree of crystallization. We therefore chose the average  $a_{\text{SiO}_2}$  of  $0.6 \pm 0.1$  for our temperature calculations. The  $a_{\text{TiO}_2}$  also shows little variation between runs with different starting compositions and does not vary with temperature. Each composition yields maximum  $a_{\text{TiO}_2}$  values between 0.1 and 0.2. However, using these low  $a_{\text{TiO}_2}$  and  $a_{\text{SiO}_2}$  values results in impossibly high Ti-in-zircon temperatures that are above the zircon saturation temperatures for our initial melt compositions, which range from 1250 to 1266 °C using the revised relationship from Boehnke et al. (2013). In order for our highest Ti concentrations to be consistent with these temperatures and with  $a_{\text{SiO}_2} = 0.6$ , our  $a_{\text{TiO}_2}$  would need to be  $\sim 0.3$ . It is interesting to note that in all MELTS runs, ilmenite ( $\text{FeTiO}_3$ ) begins to crystallize between  $\sim 980^\circ$  and 1141 °C, which is below the zircon saturation temperature suggesting some zircons may be crystallizing before ilmenite. The activity of  $a_{\text{TiO}_2}$  could therefore be higher prior to ilmenite formation, which would remove  $\text{TiO}_2$  from the melt, so a value of  $\sim 0.3$  appears reasonable for our high Ti zircons.

Based on the MELTS results and zircon saturation temperatures of KREEP-rich rocks, our best estimates for oxide activities are  $a_{\text{SiO}_2} = 0.6 \pm 0.1$  and  $a_{\text{TiO}_2} = 0.25 \pm 0.05$ . The Ti-in-zircon temperatures calculated using these values range from  $958 \pm 57$  to  $1321 \pm 100$  °C (uncertainties include the range in  $a_{\text{SiO}_2}$  and  $a_{\text{TiO}_2}$ , and  $1\sigma$  analytical error in Ti concentration). The lower bound agrees well with the dry solidus for granite at near surface pressures ( $\sim 950$  °C; Robertson and Wyllie, 1971) and the highest crystallization temperature is within error of the zircon saturation temperatures.

Our Ti concentrations are in agreement with the average Ti concentrations for zircons from Apollo 12, 14, 15, and 17 reported in Taylor et al. (2009a, 2009b), Valley et al. (2014), and Hopkins and Mojzsis (2015), although our calculated temperatures are slightly higher due to assumptions of oxide activity. However, if we recalculate the temperatures for their zircons using our new constraints on  $a_{\text{SiO}_2}$  and  $a_{\text{TiO}_2}$ , the values agree well with the temperatures reported herein. For comparison, the lunar zircon temperatures are higher than those of terrestrial Hadean zircons, which are all below 800 °C implying crystallization in hydrous magmas (Watson and Harrison, 2005; Harrison and Schmitt, 2007; Bell and Harrison, 2013).

## 6. SUMMARY AND CONCLUSIONS

The lunar zircon record has been used to infer the timing and characteristics of residual KREEP magmatism, however discrepancies exist between the crystallization ages and trace elements of lunar zircons, and the whole rock record and the LMO solidification models. In this paper we presented coordinated age and trace element analyses, which, in conjunction with microstructural imaging, address these discrepancies.

The large size of most zircon parent crystals, some in this study are over a millimeter in length, suggests formation in highly enriched KREEP magmas and not an impact environment. The distributions of  $^{207}\text{Pb}$ – $^{206}\text{Pb}$  igneous crystallization ages for zircons from Apollo 14, 15, and 17 landing sites all exhibit a peak in age around 4.33 Ga, however they differ in that only Apollo 14 samples contain a population of zircons with ages less than 4.1 Ga. We observed that the majority, 90%, of all lunar zircons are older than 4.1 Ga and primary igneous zonation was identified only in zircons  $>4.2$  Ga. Additionally, the  $<4.1$  Ga zircons from Apollo 14 are often smaller than 50  $\mu\text{m}$  and/or show evidence of open system behavior, suggesting an increased likelihood of impact alteration. Together with the age distributions, the characteristics of the young lunar zircons suggest that the majority of zircon forming KREEP magmatism ceased between 4.2 and 4.1 Ga.

We also employed microstructural analyses to identify zircons with textures indicative of impact recrystallization. Two 15455 granular texture zircons that contain micron sized baddeleyite domains yield  $^{207}\text{Pb}$ – $^{206}\text{Pb}$  ages of  $\sim 4.330$  Ga, and a third granular zircon from 14259 has a  $^{207}\text{Pb}$ – $^{206}\text{Pb}$  age of 4.20 Ga. The ages of these grains, in combination with previously proposed lunar zircon impact ages, suggest lunar zircons are recording signatures of large impact events at least every 100 Myr during the first 500 Myr of lunar history. We find no signature of a lunar cataclysm at  $\sim 3.9$  to  $\sim 3.8$  Ga in the zircons analyzed herein.

We compiled a REE dataset large enough to investigate characteristics of lunar zircon parent magmas. High-resolution electron beam imaging of the SIMS analysis spots and monitoring of Fe concentrations revealed that approximately half of the REE analyses contained contributions from inclusions (mostly impact melt), cracks, or surrounding phases. These features are often hard to avoid during SIMS analyses due to the shocked nature of the lunar grains. After we filtered for contaminated measurements, the pristine zircon analyses are characterized by one REE pattern that exhibits a negative Eu anomaly and no positive Ce anomaly. These results are consistent with zircons forming in a KREEPy, reducing parent magma. Additionally, there is no correlation between Hf and igneous crystallization age, which may suggest that either there were multiple zircon forming source regions or that some zircon ages have been slightly altered by later impact events. However the concordant behavior of most zircons in this study does not support the latter scenario.

For the purpose of Ti-in-zircon thermometry, we determined new estimates for oxide activities in the KREEP source of  $a_{\text{SiO}_2} = 0.6 \pm 0.1$  and  $a_{\text{TiO}_2} = 0.25 \pm 0.05$  using MELTS models and zircon saturation temperatures for a range of likely parent melt compositions. Using these values, we calculated Ti-in-zircon temperatures for zircons from all three landing sites ranging from  $958 \pm 57$  to  $1321 \pm 100$  °C. These values are bounded by the dry solidus temperature of granite and are within error of the zircon saturation temperatures for the estimated starting magma compositions. These temperatures are consistent with zircons forming in anhydrous conditions with little to no allowance for water in late stage KREEPy melts.

The coordinated analyses presented in this study resolved some discrepancies between the lunar whole rock record, LMO crystallization models, and the lunar zircon data. In general, our results suggest that lunar zircons formed in reduced, anhydrous parent melts, the majority of which crystallized by 4.2–4.1 Ga. Further investigations into the extent of impact disturbance in the  $<4.1$  Ga zircons and the robustness of the  $>4.37$  Ga zircon ages will help to fully reconcile the lunar whole rock and zircon histories.

## ACKNOWLEDGEMENTS

The authors would like to acknowledge T. Mark Harrison for fruitful discussions of zircon trace elements, zircon saturation, and Ti-in-zircon thermometry. We would also like to thank Beth Ann Bell, Patrick Boehnke, Matthew Wielicki, and Rita Economos for their assistance with SIMS analyses and for helpful advice about statistics and trace elements in zircons. Special thanks are also given to Dianne Taylor for her contributions and assistance with zircon separation and SIMS analyses. We also acknowledge Ivan Barker who collaborated on the EBSD microstructural analyses. This work would not have been possible if not for the generous allocation of the Apollo samples for this study by NASA CAPTEM. The authors would also like to thank Marion Grange, Steve Mojzsis, and Randy Korotev for their constructive reviews and insightful comments. This work was supported in part by the NASA Earth and Space Sciences Fellowship and the NASA Cosmochemistry program. The UCLA ion microprobe laboratory is partially supported by a grant from the NSF Instrumentation and Facilities Program. NSERC support of the UWO ZAPLab is gratefully acknowledged. This manuscript was prepared in part at Lawrence Livermore National Laboratory under Contract DE-AC52-07NA27344.

## APPENDIX A. SUPPLEMENTARY DATA

Supplementary data associated with this article can be found, in the online version, at <http://dx.doi.org/10.1016/j.gca.2016.12.019>.

## REFERENCES

- Asimow P. D. and Ghiorso M. S. (1998) Algorithmic modifications extending MELTS to calculate subsolidus phase relations. *Am. Mineral.* **83**, 1127–1132.
- Arvidson R., Drozd R., Guinness E., Hohenburg C., Morgan F., Morrison R. and Oberbeck V. (1976) Cosmic ray exposure ages of Apollo 17 samples and the age of Tycho. In *Lunar Sci. Conf. XII. Lunar Planet. Inst., Houston*, pp. 2817–2832 (abstr.).

- Bell E. A. and Harrison T. M. (2013) Post-Hadean transitions in Jack Hills zircon provenance: a signal of the Late Heavy Bombardment? *Earth Planet. Sci. Lett.* **364**, 1–11.
- Bellucci J. J., Whitehouse M. J., Nemchin A. A., Snape J. F., Pidgeon R. T., Grange M., Reddy S. M. and Timms N. (2016) A scanning ion imaging investigation into the micron-scale U–Pb systematics in a complex lunar zircon. *Chem. Geol.* **438**, 112–122.
- Belousova E. A., Griffin W. L., O'Reilly S. Y. and Fisher N. I. (2002) Igneous zircon: trace element composition as an indicator of source rock type. *Contrib. Mineral. Petrol.* **143**, 602–622.
- Bernatowicz T. J., Hohenberg C. M., Hudson B., Kennedy B. M. and Podosek F. A. (1978) Argon ages for lunar breccias 14064 and 15405. In *Lunar Sci. Conf. IX. Lunar Planet. Inst.*, Houston, pp. 905–919 (abstr.).
- Blanchard D. P., Haskin L. A., Jacobs J. W., Brannon J. C. and Korotev R. L. (1975) Major and trace element chemistry of boulder 1 at Station 2, Apollo 17. *Moon* **14**, 359–371.
- Boehnke P., Watson E. B., Trail D., Harrison T. M. and Schmitt A. K. (2013) Zircon saturation re-visited. *Chem. Geol.* **351**, 324–334.
- Bogard D. D., Garrison D. H., Shih C. Y. and Nyquist L. E. (1994) <sup>39</sup>Ar–<sup>40</sup>Ar dating of two lunar granites: the age of Copernicus. *Geochim. Cosmochim. Acta.* **58**, 3093–3100.
- Boyce J. W., Tomlinson S. M., McCubbin F. M., Greenwood J. P. and Treiman A. H. (2014) The lunar apatite paradox. *Science* **344**, 400–402.
- Braddy D., Hutcheon I. D. and Price P. B. (1975) Crystal chemistry of Pu and U and concordant fission track ages of lunar zircons and whitlockites. In *Lunar Sci. Conf. VI. Lunar Planet. Inst.*, Houston, pp. 3587–3600 (abstr.).
- Burnett D. S., Huneke J. C., Podosek F. A., Russ, III, G. P., Turner G. and Wasserburg G. J. (1972) The Irradiation History of Lunar Samples. In *Lunar Planet. Sci. III. Lunar Planet. Inst.*, Houston, pp. 105–107 (abstr.).
- Burnham A. D. and Berry A. J. (2012) An experimental study of trace element partitioning between zircon and melt as a function of oxygen fugacity. *Geochim. Cosmochim. Acta* **95**, 196–212.
- Cavosie A. J., Erickson T. M., Timms N. E., Reddy S. M., Talavera C., Montalvo S. D., Pincus M. R., Gibbon R. J. and Moser D. E. (2015) A terrestrial perspective on using ex situ shocked zircons to date lunar impacts. *Geology* **43**, 999–1002.
- Cherniak D. J., Hanchar J. M. and Watson E. B. (1997) Rare-earth diffusion in zircon. *Chem. Geol.* **134**, 289–301.
- Cherniak D. J. and Watson E. B. (2000) Pb diffusion in zircon. *Chem. Geol.* **172**, 5–24.
- Church S. E., Tilton G. R. and Chen J. H. (1976) Lead isotopic studies of lunar soils: Their bearing on the time scale of agglutinate formation. In *Lunar Sci. Conf. VII. Lunar Planet. Inst.*, Houston, pp. 351–371 (abstr.).
- Claiborne L. L., Miller C. F. and Wooden J. L. (2010) Trace element composition of igneous zircon: a thermal and compositional record of the accumulation and evolution of a large silicic batholith, Spirit Mountain, Nevada. *Contrib. Mineral. Petrol.* **160**, 511–531.
- Crow C. A., Crowther S. A., Gilmour J. D., Busemann H., Moser D. E. and McKeegan K. D. (2015) U–Xe degassing ages of terrestrial and lunar impact zircons. In *78th Meteor. Soc. Meet.*, Meteor. Soc., Berkeley, #5226 (abstr.).
- Dalrymple G. B. and Ryder G. (1996) <sup>40</sup>Ar–<sup>39</sup>Ar age spectra of Apollo 17 highlands breccia samples by laser step heating and the age of the Serenitatis basin. *J. Geophys. Res.* **101**, 26069–26084.
- Davidson A. and van Breeman O. (1988) Baddeleyite-zircon relationships in coronitic metagabbro, Grenville Province, Ontario: implications for geochronology. *Contrib. Mineral. Petrol.* **100**, 291–299.
- Dence M. R. and Plant A. G. (1972) Analysis of Fra Mauro samples and the origin of the Imbrium Basin. *Lunar Sci. Conf. III. Lunar Planet. Inst.*, Houston, 379–399 (abstr.).
- Deutsch A. and Stöffler D. (1987) Rb–Sr-analyses of Apollo 16 melt rocks and a new age estimate for the Imbrium basin: Lunar basin chronology and the early heavy bombardment of the moon. *Geochim. Cosmochim. Acta* **51**, 1951–1964.
- Dickinson J. E. and Hess P. C. (1982) Zircon saturation in lunar basalts and granites. *Earth Planet. Sci. Lett.* **57**, 336–344.
- Drozdz R., Hohenberg C., Morgan C. and Ralston C. (1974) Cosmic-ray exposure history at the Apollo 16 and other lunar sites: lunar surface dynamics. *Geochim. Cosmochim. Acta* **38**, 1625–1642.
- Eberhardt P., Geiss J., Grögler N. and Stettler A. (1973) How old is the crater Copernicus? *The Moon* **8**, 104–114.
- Elkins Tanton L. T., Van Orman J. A., Hager B. H. and Grove T. L. (2002) Re-examination of the lunar magma ocean cumulate overturn hypothesis: melting or mixing is required. *Earth Planet. Sci. Lett.* **196**, 239–249.
- Elkins-Tanton L. T., Burgess S. and Yin Q. Z. (2011) The lunar magma ocean: reconciling the solidification process with lunar petrology and geochronology. *Earth Planet. Sci. Lett.* **304**, 326–336.
- Von Engelhardt W., Arndt J., Stöffler D. and Schneider H. (1972) Apollo 14 regolith and fragmental rocks, their compositions and origin by impacts. In *Lunar Sci. Conf. III. Lunar Planet. Inst.*, Houston, pp. 753–770 (abstr.).
- Eugster O., Eberhardt P., Geiss J., Grogler N., Jungck M., Meier F., Morgell and Niederer F. (1984) Cosmic Ray Exposure Histories of Apollo 14, Apollo 15, and Apollo 16 Rocks. In *Lunar Planet. Sci. XIV*, pp. B498–B512 (abstr.).
- Ferriss E. D. A., Essene E. J. and Becker U. (2007) Computational study of the effect of pressure on the Ti-in-zircon thermometer. *Eur. J. Mineral.* **20**, 745–755.
- Ferry J. M. and Watson E. B. (2007) New thermodynamic models and revised calibrations for the Ti-in-zircon and Zr-in-rutile thermometers. *Contrib. Mineral. Petrol.* **154**, 429–437.
- Fields P. R., Diamond H., Metta D. N. and Rokop D. J. (1973) Reaction products of lunar uranium and cosmic rays. In *Lunar Sci. Conf. IV. Lunar Planet. Inst.*, Houston, pp. 2123–2130 (abstr.).
- Fu B., Page Z. F., Cavosie A. J., Fournelle J., Kita N. T., Lackey J. S., Wilde S. A. and Valley J. W. (2008) Ti-in-zircon thermometry: applications and limitations. *Contrib. Mineral. Petrol.* **156**, 197–215.
- Garver J. I. and Kamp P. J. J. (2002) Integration of zircon color and zircon fission-track zonation patterns in orogenic belts: application to the Southern Alps, New Zealand. *Tectonophysics* **349**, 203–219.
- Ghiorsso M. S. and Sack R. O. (1995) Chemical mass transfer in magmatic processes. IV. A revised and internally consistent thermodynamic model for the interpolation and extrapolation of liquid–solid equilibria in magmatic systems at elevated temperatures and pressures. *Contrib. Mineral. Petrol.* **119**, 197–212.
- Gibson R. L., Armstrong R. A. and Reimold W. U. (1997) The age and thermal evolution of the Vredefort impact structure: a single-grain U–Pb zircon study. *Geochim. Cosmochim. Acta* **61**, 1531–1540.
- Grange M. L., Nemchin A. A., Pidgeon R. T., Timms N., Muhling J. R. and Kennedy A. K. (2009) Thermal history recorded by the Apollo 17 impact melt breccia 73217. *Geochim. Cosmochim. Acta* **73**, 3093–3107.

- Grange M. L., Nemchin A. A., Timms N., Pidgeon R. T. and Meyer C. (2011) Complex magmatic and impact history prior to 4.1 Ga recorded in zircon from Apollo 17 South Massif aphanitic breccia 73235. *Geochim. Cosmochim. Acta* **75**, 2213–2232.
- Grange M. L., Pidgeon R. T., Nemchin A. A., Timms N. E. and Meyer C. (2013a) Interpreting U–Pb data from primary and secondary features in lunar zircon. *Geochim. Cosmochim. Acta* **101**, 112–132.
- Grange M. L., Nemchin A. A. and Pidgeon R. T. (2013b) The effect of 1.9 and 1.4 Ga impact events on 4.3 Ga zircon and phosphate from an Apollo 15 melt breccia. *J. Geophys. Res. Planet.* **118**, 2180–2197.
- Grieve R. A., McKay G. A., Smith H. D. and Weill D. F. (1975) Lunar polymict breccia 14321: a petrographic study. *Geochim. Cosmochim. Acta* **39**, 229–245.
- Grimes C. B., John B. E., Kelemen P. B., Mazdab F. K., Wooden J. L., Cheadle M. J., Hanghøj K. and Schwartz J. J. (2007) Trace element chemistry of zircons from oceanic crust: a method for distinguishing detrital zircon provenance. *Geology* **35**, 643–646.
- Harrison T. M. and Schmitt A. K. (2007) High sensitivity mapping of Ti distributions in Hadean zircons. *Earth Planet. Sci. Lett.* **261**, 9–19.
- Heiken G., Vaniman D. and French B. M. (1991) *Lunar Sourcebook: A User's Guide to the Moon*. Cambridge University Press.
- Hinton R. and Upton B. G. (1991) The chemistry of zircon: variations within and between large crystals from syenite and alkali basalt xenoliths. *Geochim. Cosmochim. Acta* **55**, 3287–3302.
- Hinton R. W. and Meyer C. (1991) Ion probe analysis of zircon and ytrobetafite in a lunar granite. In *Lunar Planet. Sci. Conf. XXII*. Lunar Planet. Inst., Houston, pp. 575–576 (abstr.).
- Hopkins M. D. and Mojzsis S. J. (2015) A protracted timeline for lunar bombardment from mineral chemistry, Ti thermometry and U–Pb geochronology of Apollo 14 melt breccia zircons. *Contrib. Mineral. Petrol.* **169**, 30.
- Hoskin P. W. O. and Ireland T. R. (2000) Rare earth element chemistry of zircon and its use as a provenance indicator. *Geology* **28**, 627–630.
- Hoskin P. W. O. and Schaltegger U. (2003) The composition of zircon and igneous and metamorphic petrogenesis. *Rev. Mineral. Geochem.* **53**, 27–62.
- Kaiser A., Lobert M. and Telle R. (2008) Thermal stability of zircon (ZrSiO<sub>4</sub>). *J. Eur. Ceram. Soc.* **28**, 2199–2211.
- Kleinmann B. (1969) The breakdown of zircon observed in the libyan desert glass as evidence of its impact origin. *Earth Planet. Sci. Lett.* **5**, 497–501.
- Korotev R. L. (1987) Mixing levels, the apennine front soil component, and compositional trends in the apollo 15 soils. In *Lunar Planet. Sci. Conf. VII*. Lunar Planet. Inst., Houston, pp. E411–E431 (abstr.).
- Kovaleva E., Klötzli U., Habler G. and Libowitzky E. (2014) Finite lattice distortion patterns in plastically deformed zircon grains. *Solid Earth* **5**, 1099–1122.
- Kring D. A., McGovern P. J., Potter R. W. K., Collins G. S., Grange M. L. and Nemchin A. A. (2015) Was an epoch of lunar magmatism triggered by the south pole-aitken basin impact? In *Earth Solar System Impact Bombard. III*. Lunar Planet. Inst., Houston, p. 3009 (abstr.).
- Krogh T. E., Kamo S. L. and Bohor B. F. (1993) Fingerprinting the K/T impact site and determining the time of impact by U–Pb dating of single shocked zircons from distal ejecta. *EPSL*, 425–429.
- Labotka T. C., Kempa M. J., White C., Papike J. J. and Laul J. C. (1980) The lunar regolith: comparative petrology of the Apollo sites. In *Lunar Planet. Sci. Conf. XI*. Lunar Planet. Inst., Houston, pp. 1285–1305 (abstr.).
- Liu D., Jolliff B. L., Zeigler R. A., Korotev R. L., Wan Y., Xie H., Zhang Y., Dong C. and Wang W. (2012) Comparative zircon U–Pb geochronology of impact melt breccias from Apollo 12 and lunar meteorite SaU 169, and implications for the age of the Imbrium impact. *Earth Planet. Sci. Lett.* **319–320**, 277–286.
- Lovering J. F., Wark D. A., Gleadow A. J. W. and Sewell D. K. B. (1972) Uranium and potassium fractionation in pre-Imbrian lunar crustal rocks. In *Lunar Sci. Conf. III*. Lunar Planet. Inst., Houston, pp. 281–294 (abstr.).
- LSPET (1973) Apollo 17 lunar samples: chemical and petrographic descriptions. *Science* **182**, 659–672.
- Lucchitta B. K. (1977) Crater clusters and light mantle at the apollo 17 site; a results of secondary impact from Tycho. *Icarus* **30**, 80–96.
- Ludwig K. R. (1980) Calculation of uncertainties of U–Pb isotope data. *EPSL* **46**, 212–220.
- Lugmair G. W. and Marti K. (1972) Neutron and spallation effects in fra mauro regolith. In *Lunar Planet. Sci. Conf. III*. Lunar Planet. Inst., Houston, pp. 495–496 (abstr.).
- Mann H. B. and Whitney D. R. (1947) On a test of whether one of two random variables is stochastically larger than the other. *Ann. Math. Stat.* **18**, 50–60.
- McDonough W. F. and Sun S.-S. (1995) The composition of the Earth. *Chem. Geol.* **120**, 223–253.
- McGee P. E., Simonds C. H., Warner J. L. and Phinney W. C. (1979) *Introduction to the Apollo Collection: Part II. Lunar Breccias*. NASA STI Program.
- McKay D. S., Heiken G. H., Taylor R. M., Clanton U. S., Morrison D. A. and Ladle G. H. (1972) Apollo 14 soils: size distribution and particle types. In *Lunar Sci. Conf. III*. Lunar Planet. Inst., Houston, pp. 983–994 (abstr.).
- Merle R. E., Nemchin A. A., Grange M. L., Whitehouse M. J. and Pidgeon R. T. (2014) High resolution U–Pb ages of Ca-phosphates in Apollo 14 breccias: Implications for the age of the Imbrium impact. *Meteorit. Planet. Sci.* **49**, 2241–2251.
- Meyer C., Brett R., Hubbard N. J., Morrison D. A., McKay D. S., Aitken F. K., Takeda H. and Schonfeld E. (1971) Mineralogy, chemistry, and origin of the KREEP component in soil samples from the Ocean of Storms. In *Lunar Sci. Conf. II*. Lunar Planet. Inst., Houston, pp. 393–411 (abstr.).
- Meyer C., Williams I. S. and Compston W. (1989) <sup>207</sup>Pb–<sup>206</sup>Pb Ages of zircon-containing rock fragments indicate continuous magmatism in the lunar crust from 4350 to 3900 million years. In *Lunar Planet. Sci. Conf. XII*. Lunar Planet. Inst., Houston, pp. 691–692 (abstr.).
- Meyer C., Williams I. S. and Compston W. (1996) Uranium-lead ages for lunar zircons: Evidence for a prolonged period of granophyre formation from 4.32 to 3.88 Ga. *Meteorit. Planet. Sci.* **387**, 370–387.
- Meyer J., Elkins-Tanton L. and Wisdom J. (2010) Coupled thermal–orbital evolution of the early Moon. *Icarus* **208**, 1–10.
- Mezger K. and Krogstad E. (1997) Interpretation of discordant U–Pb zircon ages: an evaluation. *J. Metamorph. Geol.* **15**, 127–140.
- Mojzsis S. J., Devaraju T. C. and Newton R. C. (2003) Ion Microprobe U–Pb age determinations on zircon from the late archean granulite facies transition zone of Southern India. *J. Geol.* **111**, 407–425.
- Morris R. V. (1978) The surface exposure (maturity) of lunar soils: Some concepts and Is/FeO compilation. In *Lunar Planet. Sci. Conf. IX*. Lunar Planet. Inst., Houston, pp. 2287–2297 (abstr.).
- Moser D. E. (1997) Dating the shock wave and thermal imprint of the giant Vrederfort impact, South Africa. *Geology* **25**, 7–10.
- Moser D. E., Cupelli C. L., Barker I. R., Flowers R. M., Bowman J. R., Wooden J. and Hart J. R. (2011) New zircon shock

- phenomena and their use for dating and reconstruction of large impact structures revealed by electron nanobeam (EBSD, CL, EDS) and isotopic U–Pb and (U–Th)/He analysis of the Vredefort dome. *Can. J. Earth Sci.* **48**, 117–139.
- Nemchin A. A., Whitehouse M. J., Pidgeon R. T. and Meyer C. (2006) Oxygen isotopic signature of 4.4–3.9 Ga zircons as a monitor of differentiation processes on the Moon. *Geochim. Cosmochim. Acta* **70**, 1864–1872.
- Nemchin A. A., Pidgeon R. T., Whitehouse M. J., Vaughan J. P. and Meyer C. (2008) SIMS U–Pb study of zircon from Apollo 14 and 17 breccias: Implications for the evolution of lunar KREEP. *Geochim. Cosmochim. Acta* **72**, 668–689.
- Nemchin A. A., Timms N., Pidgeon R., Geisler T., Reddy S. and Meyer C. (2009) Timing of crystallization of the lunar magma ocean constrained by the oldest zircon. *Nat. Geosci.* **2**, 133–136.
- Nemchin A. A., Grange M. L. and Pidgeon R. T. (2010) Distribution of rare earth elements in lunar zircon. *Am. Mineral.* **95**, 273–283.
- Norman M. D. and Nemchin A. A. (2014) A 4.2 billion year old impact basin on the Moon: U–Pb dating of zirconolite and apatite in lunar melt rock 67955. *Earth Planet. Sci. Lett.* **388**, 387–398.
- Paces J. B. and Miller J. D. (1993) Precise U–Pb ages of duluth complex and related mafic intrusions, northeastern Minnesota: geochronological insights to physical, petrogenetic, paleomagnetic, and tectonomagmatic processes associated with the 1.1 Ga midcontinent rift system. *J. Geophys. Res.* **98**, 13997–14013.
- Palme H., Baddenhausen H., Blum K., Cendales M., Dreibus G., Hofmeister H., Kruse H., Palme C., Spettel B., Vilcek E. and Wanke H. (1978) New data on lunar samples and achondrites and a comparison of the least fractionated samples from the earth, the moon and the eucrite parent body. In *Lunar Planet. Sci. Conf. IX*. Lunar Planet. Inst., Houston, pp. 25–57 (abstr.).
- Pidgeon R. T., Nemchin A. A., van Bronswijk W., Geisler T., Meyer C., Compston W. and Williams I. S. (2007) Complex history of a zircon aggregate from lunar breccia 73235. *Geochim. Cosmochim. Acta* **71**, 1370–1381.
- Rice W. R. (1989) Analyzing tables of statistical tests. *Evolution* **43**, 223–225.
- Renne P. R., Balco G., Ludwig K. R., Mundil R. and Min K., et al. (2011) Response to the comment by W. H. Schwarz, on “Joint determination of 40K decay constants and 40Ar\*/40K for the Fish Canyon sanidine standard, and improved accuracy for 40Ar/39Ar geochronology” by P.R. Renne et al. (2010). *Geochim. Cosmochim. Acta* **75**, 5097–5100.
- Robertson J. K. and Wyllie P. J. (1971) Rock–water systems, with special reference to the water-deficient region. *Am. J. Sci.* **271**, 252–277.
- Ryder G. (1976) Lunar sample 15405: remnant of a KREEP basalt–granite differentiated pluton. *EPSL* **29**, 255–268.
- Sañudo-Wilhelmy S. A. and Flegal A. R. (1994) Temporal variations in lead concentrations and isotopic composition in the Southern California Bight. *Geochim. Cosmochim. Acta* **58**, 3315–3320.
- Schmieder M., Tohver E., Jourdan F., Denyszyn S. W. and Haines P. W. (2015) Zircons from the Acraman impact melt rock (South Australia): Shock metamorphism, U–Pb and <sup>40</sup>Ar/<sup>39</sup>Ar systematics, and implications for the isotopic dating of impact events. *Geochim. Cosmochim. Acta* **161**, 71–100.
- Schmitt A. K. and Zack T. (2012) High-sensitivity U–Pb rutile dating by secondary ion mass spectrometry (SIMS) with an O<sup>2+</sup> primary beam. *Chem. Geol.* **332–333**, 65–73.
- Shih C.-Y., Bansal B. M., Wiesmann H., Nyquist L. E. and Bogard D. D. (1986) Geochronology and petrogenesis of Apollo 14 very high potassium mare basalts. In *Lunar Planet. Sci. Conf. XVI*. Lunar Planet. Inst., Houston, pp. D214–D228 (abstr.).
- Shih C.-Y., Nyquist L., Bogard D., Dasch E., Bansal B. and Wiesmann H. (1987) Geochronology of high-K aluminous mare basalt clasts from Apollo 14 breccia 14304. *Geochim. Cosmochim. Acta* **51**, 3255–3271.
- Shih C.-Y., Nyquist L., Dasch E., Bogard D., Bansal B. and Wiesmann H. (1993) Ages of pristine noritic clasts from lunar breccias 15445 and 15455. *Geochim. Cosmochim. Acta* **57**, 915–931.
- Shih C.-Y., Nyquist L. E., Bansal B. M. and Wiesmann H. (1992) Rb–Sr and Sm–Nd chronology of an Apollo 17 KREEP basalt. *Earth Planet. Sci. Lett.* **108**, 203–215.
- Simon S. B. and Papike J. J. (1981) The Lunar regolith: comparative petrology of the Apollo and Luna soils. In *Lunar Planet. Sci. Conf. XIIB*. Lunar Planet. Inst., Houston, pp. 984–986 (abstr.).
- Simonds C. H., Phinney W. C., Warner J. L., McGee P. E., Geelsin J., Brown R. W. and Rhodes J. M. (1977) Apollo 14 revisited, or breccias aren’t so bad after all. In *Lunar Sci. Conf. VIII*. Lunar Planet. Inst., Houston, pp. 1869–1893 (abstr.).
- Smith J. M., Meyer C., Compston W. and Williams I. S. (1986) 73235,82 (Pomegranate): An assemblage of Lunar Zircon with unique overgrowth. In *Lunar Planet. Sci. Conf. XVII*. Lunar Planet. Inst., Houston, pp. 805–806 (abstr.).
- Snyder G. A., Taylor L. A. and Halliday A. N. (1995) Chronology and petrogenesis of the lunar highlands alkali suite: Cumulates from KREEP basalt crystallization. *Geochim. Cosmochim. Acta* **59**, 1185–1203.
- Stadermann F. J., Heusser E., Jessberger E. K., Lingner S. and Stöfler D. (1991) The case for a younger Imbrium basin: new 40Ar–39Ar ages of Apollo 14 rocks. *Geochim. Cosmochim. Acta* **55**, 2339–2349.
- Stöfler D. and Ryder G. (2001) Stratigraphy and isotope ages of lunar geologic units: chronological standard for the inner solar system. In *Chronology and Evolution of Mars* (eds. R. Kallenbach, J. Geiss and W. K. Hartmann). Springer, Netherlands, pp. 9–54.
- Swann G. A., Bailey N. G., Batson R. M., Eggelton R. E., Hait M. H., Holt H. E., Larson K., McEwen M. C., Mitchell E. D., Schaber G. G., Schafer J. P., Shepard A. B., Sutton R. L., Trask N. J., Ulrich G. E., Wilshire H. G. and Wolfe E. W. (1971) Preliminary geologic investigation of the Apollo 14 landing site. In *Apollo 14 Preliminary Science Report Nasa Sp-272*, pp. 39–85.
- Swann G. A., Bailey N. G., Batson R. M., Freeman V. L., Hait M. H., Head J. W., Holt H. E., Howard K. A., Irwin J. B., Larson K. B., Muehlberger W. R., Reed V. S., Rennison J. J., Schaber G. G., Scott D. R., Silver L. T., Sutton R. L., Ulrich G. E., Wilshire H. G. and Wolfe E. W. (1972) Preliminary geologic investigation of the Apollo 15 landing site. In *Apollo 15 Preliminary Science Report NASA SP-289*.
- Swann G. A., Bailey N. G., Batson R. M., Eggelton R. E., Hait M. H., Holt H. E., Larson K. B., Reed V. S., Schaber G. G., Sutton R. L., Trask N. J., Ulrich G. E. and Wilshire H. G. (1977) *Geology of the Apollo 14 landing site in the Fra Mauro Highlands*. Geological Survey Professional Paper **880**.
- Taylor D. J., McKeegan K. D. and Harrison T. M. (2009a) Lu–Hf zircon evidence for rapid lunar differentiation. *Earth Planet. Sci. Lett.* **279**, 157–164.
- Taylor D. J., McKeegan K. D., Harrison T. M. and Young E. D. (2009b) Early differentiation of the lunar magma ocean – new Lu–Hf isotope results from Apollo 17. *Geochim. Cosmochim. Acta Suppl.* **73**, A1317.
- Taylor G. J., Warner R. D., Keil K., Ma M.-S. and Schmitt R. A. (1980) Silicate liquid immiscibility, evolved lunar rocks and the

- formation of KREEP. In *Conf. Lunar Highlands Crust*. Lunar Planet. Inst., Houston, pp. 339–352 (abstr.).
- Taylor L. A., Shervais J. W., Hunter R. H., Shih C.-Y., Bansal B. M., Wooden J., Nyquist L. E. and Laul L. C. (1983) Pre-4.2 AE mare-basalt volcanism in the lunar highlands. *Earth Planet. Sci. Lett.* **66**, 33–47.
- Timms N. E., Reddy S. M., Healy D., Nemchin A. A., Grange M. L., Pidgeon R. T. and Hart R. (2012) Resolution of impact-related microstructures in lunar zircon: A shock-deformation mechanism map. *Meteorit. Planet. Sci.* **47**, 120–141.
- Trail D., Watson E. B. and Tailby N. D. (2012) Ce and Eu anomalies in zircon as proxies for the oxidation state of magmas. *Geochim. Cosmochim. Acta* **97**, 70–87.
- Valley J. W., Spicuzza M. J. and Ushikubo T. (2014) Correlated  $\delta^{18}\text{O}$  and [Ti] in lunar zircons: a terrestrial perspective for magma temperatures and water content on the Moon. *Contrib. to Mineral. Petrol.* **167**, 956.
- Wadhwa M. (2008) Redox Conditions on Small Bodies, the Moon and Mars. *Rev. Mineral. Geochem.* **68**, 493–510.
- Wanke H., Baddenhausen H., Balacesu A., Teschke F., Spettel B., Dreibus G., Palme H., Quijano-Rico M., Kruse H., Wlotzka F. and Begemann F. (1972) ultielement analyses of lunar samples and some implications of the results. In *Lunar Sci. Conf III*. Lunar and Planet. Inst., Houston, pp. 1251–1268 (abstr.).
- Warren P. H., Taylor G. J., Keil K., Marshall C. and Wasson J. T. (1981) Foraging westward for pristine nonmare rocks: Complications from petrogenetic models. In *Lunar Planet. Sci. Conf. XIIB*. Lunar and Planet. Inst., Houston, pp. 21–40 (abstr.).
- Warren P. H. and Wasson J. T. (1979) The origin of KREEP. *Rev. Geophys. Sp. Phys.* **17**, 73–88.
- Watson E. B. and Harrison T. M. (2005) Zircon thermometer reveals minimum melting conditions on earliest Earth. *Science* **308**, 841–844.
- Wiedenbeck M., Hanchar J. M., Peck W. H., Sylvester P., Valley J., Whitehouse M., Kronz A., Morishita Y., Nasdala L., Fiebig J., Franchi I., Girard J.-P., Greenwood R. C., Hinton R., Kita N., Mason P. R. D., Norman M., Ogasawara M., Piccoli R., Rhede D., Satoh H., Schulz-Dobrick B., Skar O., Spicuzza M. J., Terada K., Tindle A., Togashi S., Vennemann T., Xie Q. and Zheng Y.-F. (2004) Further characterisation of the 91500 Zircon Crystal. *Geostand. Geoanalytical Res.* **28**, 9–39.
- Wielicki M. M., Harrison T. M. and Schmitt A. K. (2012) Geochemical signatures and magmatic stability of terrestrial impact produced zircon. *Earth Planet. Sci. Lett.* **321–322**, 20–31.
- Wilshire H. G. and Jackson E. D. (1972) Petrology and stratigraphy of the Fra Mauro formation at the apollo 14 site. *Geol. Surv. Prof. Pap.* **785**.
- Wopenka B., Jolliff B. L., Zinner E. and Kremser D. T. (1996) Trace element zoning and incipient metamictization in a lunar zircon: Application of three microprobe techniques. *Am. Mineral.* **81**, 902–912.
- Zhang A. C., Taylor L. A., Wang R. C., Li Q. L., Li X. H., Patchen A. D. and Liu Y. (2012) Thermal history of Apollo 12 granite and KREEP-rich rock: Clues from Pb/Pb ages of zircon in lunar breccia 12013. *Geochim. Cosmochim. Acta* **95**, 1–14.

Associate editor: Maud Boyet